Review

Siqi Yan, Xiaolong Zhu, Jianji Dong, Yunhong Ding* and Sanshui Xiao*

2D materials integrated with metallic nanostructures: fundamentals and optoelectronic applications

https://doi.org/10.1515/nanoph-2020-0074
Received January 31, 2020; revised March 5, 2020; accepted March 5, 2020

Abstract: Due to their novel electronic and optical properties, atomically thin layered two-dimensional (2D) materials are becoming promising to realize novel functional optoelectronic devices including photodetectors, modulators, and lasers. However, light–matter interactions in 2D materials are often weak because of the atomic-scale thickness, thus limiting the performances of these devices. Metallic nanostructures supporting surface plasmon polaritons show strong ability to concentrate light within subwavelength region, opening thereby new avenues for strengthening the light–matter interactions and miniaturizing the devices. This review starts to present how to use metallic nanostructures to enhance light–matter interactions in 2D materials, mainly focusing on photoluminescence, Raman scattering, and nonlinearities of 2D materials. In addition, an overview of ultraconfined acoustic-like plasmons in hybrid graphene–metal structures is given, discussing the nonlocal response and quantum mechanical features of the graphene plasmons and metals. Then, the review summarizes the latest development of 2D material–based optoelectronic devices integrated with plasmonic nanostructures. Both off-chip and on-chip devices including modulators and photodetectors are discussed. The potentials of hybrid 2D materials plasmonic optoelectronic devices are finally summarized, giving the future research directions for applications in optical interconnects and optical communications.

Keywords: two-dimensional materials; plasmonic nanostructures; optoelectronic devices.

1 Introduction

The research on two-dimensional (2D) materials, including graphene and transition metal dichalcogenides (TMDCs), has been significantly boosting. More recently, a computational 2D database obtained by state-of-the-art density functional theory and many-body perturbation theory shows that more than 1500 of new potentially synthesizable 2D materials targeting optoelectronic applications have been identified [1], stimulating the development of new fabrication technology, that is, from mechanical exfoliation [2], liquid exfoliation [3, 4], and epitaxial growth [5–8], to van der Waals (vdWs) integration [9, 10]. Latest development with respect to the stacking technique with a controllable twisted angle opens an alternative way to modulate electronic and optical properties. For example, it was demonstrated that twisted bilayer graphene can exhibit alternating superconducting and insulating regions [11, 12] and that the Moiré excitons were found in vdWs heterostructures [13]. By adjusting the twist angle, the interlayer exciton emission around 1 eV was observed from MoS_2/WSe_2 heterostructures [14–16], paving a promising way to realize ultrafast and low-threshold nanolaser for silicon (Si) photonics and optical communication system [17, 18]. Moreover, as a new member of 2D material

***Corresponding authors: Yunhong Ding,** Department of Photonics Engineering, Technical University of Denmark, DK-2800 Kongens Lyngby, Denmark; and Center for Silicon Photonics for Optical Communications, Technical University of Denmark, DK-2800 Kongens Lyngby, Denmark, e-mail: yudin@fotonik.dtu.dk; and **Sanshui Xiao,** Department of Photonics Engineering, Technical University of Denmark, DK-2800 Kongens Lyngby, Denmark; and Center for Nanostructured Graphene, Technical University of Denmark, DK-2800 Kongens Lyngby, Denmark, e-mail: saxi@fotonik.dtu.dk. https://orcid.org/0000-0001-6529-5047
Siqi Yan: Department of Photonics Engineering, Technical University of Denmark, DK-2800 Kongens Lyngby, Denmark; and Center for Silicon Photonics for Optical Communications, Technical University of Denmark, DK-2800 Kongens Lyngby, Denmark
Xiaolong Zhu: Department of Health Technology, Technical University of Denmark, DK-2800 Kongens Lyngby, Denmark
Jianji Dong: Wuhan National Laboratory for Optoelectronics, Huazhong University of Science and Technology, 430074 Wuhan, China. https://orcid.org/0000-0002-1852-8650

family, 2D perovskites [19] has also been widely combined with integrated photonic devices, such as solar cells [20, 21] and light sources [22, 23]. These developed techniques enable us to study novel fundamental physics in these newly developed 2D and vdWs heterostructures, as well as investigating their potential applications in energy harvesting [24–27], photonics and optoelectronics [28–35], and biotechnologies [36–41].

Due to the unique feature of atomic thickness, light–matter interactions in 2D materials are generally weak. One of the promising ways to increase the light–matter interactions in 2D materials is to utilize the polaritonic excitation [42–49]. The polaritonic waves, that is, plasmon polaritons [50], phonon polaritons [51, 52], and hybrid exciton polaritons [53–56], are characterized by extremely small polaritonic wavelength associated with strong optical confinement, giving rise to strong light–matter interactions. For more details, there are a few review articles discussing 2D polaritons [42, 43, 57]. However, most 2D polaritons exist at the mid-infrared window, thus resulting in the challenge to be exploited for the optoelectronic applications in the visible or near-infrared window. An alternative way to enhance the light–matter interaction is to integrate 2D materials with conventional plasmonic nanostructures based on noble metals. These metallic nanostructures support surface plasmon polaritons (SPPs), which are the collective oscillation of electrons. Due to the inherent subwavelength nature of SPPs, it can accumulate the optical energy on the nanoscale [58], thus dramatically enhancing various light–matter interaction processes including fluorescence [59–61], Raman scattering [62, 63], photocatalysis [64–66], nonlinear optical (NLO) conversion [67–70], ultrafast optics [71, 72], and solar energy harvesting [73–75]. Moreover, SPPs can be laterally confined below the diffraction limit using subwavelength metal nanostructures [76], paving the way for the miniaturization of optoelectronic devices [77–80]. The miniaturization of the optoelectronic devices results in high-density integration of photonic circuits [81–83], while having low-power consumption and high-speed signal processing.

This review presents an overview of recent study of 2D materials plasmonic hybrid systems, particularly focusing on fundamentals and optoelectronic applications, see Figure 1. One of the main questions that we will address in this review is how to use plasmonic nanostructures to enhance the light–matter interactions in 2D materials and to improve the performance of 2D material–based optoelectronic devices.

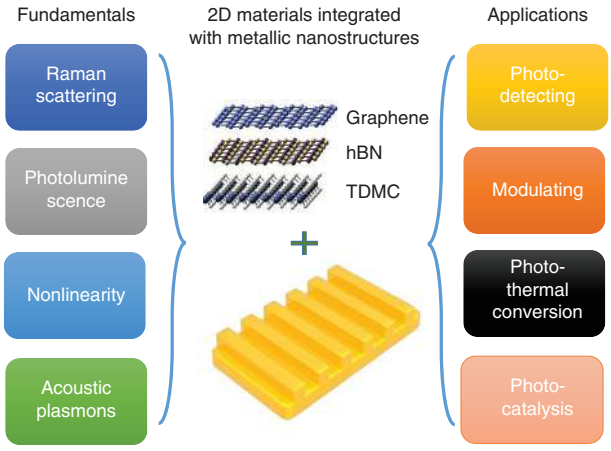

Figure 1: Schematic of 2D materials integrated with metallic nanostructures from fundamentals to applications.

2 Enhancing light–matter interactions in 2D materials by use of metallic nanostructures

Two-dimensional materials offer several attractive advantages, including tunable bandgaps, large binding energies, and strong excitonic resonances, which have been demonstrated for potential applications in biochemical sensing and imaging, semiconductors industry, and ultrafast optoelectronics for optical communication. Most 2D material–based optoelectronic devices suffer from the inherently weak interaction between pristine 2D-layered films and light. For instance, a single layer of graphene can only absorb 2.3% light at normal incidence, defined solely by the fine structure constant [84], therefore imposing substantial challenges and restrictions for many electro-optical and all-optical applications. Surface plasmon, excited by incident light [85], is the collective motion of the free electrons in metal. Because the resonance frequency of surface plasmon is sensitive to the density of the influenced free electrons at the boundaries, engineering nanostructures of those metals together with their environment provides an easy tailoring method of plasmons crossing the visible band. The combination of 2D materials with integrated plasmonic nanostructures is currently being explored for strong light–matter interactions, providing great potential in the realization of high-performance optoelectronic devices [82].

In this section, we present an overview of strong light–matter interactions in 2D materials enhanced by use of plasmonic nanostructures. Here we mainly focus on the

near-field enhancement of 2D materials in the weak coupling regime, that is, plasmon-enhanced Raman scattering, and plasmon-enhanced photoluminescence (PL) and nonlinearity. Additionally, we review recent study of ultra-confined acoustic-like plasmons in hybrid 2D-dielectric-metal structures, discussing the nonlocal response and quantum mechanical features of the graphene plasmons and metals.

2.1 Raman scattering of 2D materials enhanced by plasmonic nanostructures

Raman spectroscopy is a nondestructive technique for chemical sensing and mapping of 2D materials, which typically has a very weak signal. Since the discovery of surface-enhanced Raman spectroscopy (SERS) in the early 1970s [86], a variety of plasmonic nanostructured materials have been employed as surface SERS substrates. It is shown that the electromagnetic enhancement dominating in the measured SERS enhancement factor approximately follows the fourth power of the local electric field enhancement [62, 63]. Two-dimensional materials exhibit flat surfaces without dangling bonds, which are thought to be strong candidates for fundamental studies of Raman enhancement effect. For instance, graphene's electronic structure can be uniquely captured in its Raman spectrum, which allows high-throughput and nondestructive identification of graphene layers [87], and Raman spectroscopy is widely explored to identify the quality and the number of layers in 2D materials.

As an example of enhanced light–matter interaction, the SERS of 2D materials, such as graphene, can be modified tremendously by plasmonic nanostructures. The strong plasmon-induced enhancement of the Raman signal of graphene is due to the enhanced near-field interaction between graphene itself and the plasmonic modes [88–91]. This interaction results in an increase in absolute light absorption of 30% with up to 700-fold enhancement of the Raman response of the graphene, as shown in Figure 2A [88]. It has been shown that developing a flat 2D surface for Raman enhancement has promising importance for the further applications of SERS [89, 93]. As most 2D materials provide a good choice as an ideal flat substrate, the hybrid 2D materials–plasmonic structure is also with potential for use as Raman enhancement substrates (Figure 2A) [88]. Tip-enhanced Raman spectroscopy, where the enhancement of Raman scattering occurs near the atomically sharp pin [94], has been used for chemical imaging at the single-molecule level [95]. Quantum mechanical effects, such as electron tunneling and nonlocal screening, become extremely important especially when the distance between the tip and material approaches the subnanometer length scale, which are beyond the classical picture for the nanogap plasmons [96]. As shown in Figure 2B and C, Chen et al. [92] used layered MoS_2 as a 2D atomic crystal probe in nanoparticle-on-mirror nanoantennas to measure the plasmonic enhancement in the gap by quantitative surface-enhanced Raman scattering. For a subnanometer gap, the probable emergence of quantum mechanical effects renders an average electric field enhancement lower than classical predictions. The SERS system of 2D nanoplatelets sandwiched between a gold (Au) nanoparticle and an Au surface can also reveal a phonon doublet arising from oscillations perpendicular to and within the platelet plane [97]. The SERS detection from the combination of extreme plasmonic confinement and ultrathin layers opens the potential to excite and probe local light–matter interactions within and in neighboring plasmonic structures, which may provide a new way for further exploring quantum plasmonics.

2.2 Enhancing PL of 2D materials by plasmonic nanostructures

Transition metal dichalcogenides have attracted increasing attention due to their strong light emission, indirect-to-direct bandgap transition, and spin and valley degrees of freedom. The electronic band of TMDCs or their layered stacks is strongly influenced by the atomic compositions, the number of 2D layers, and the rotational or vertical stack of layers. As an example, when bulk MoS_2 is thinned to a monolayer structure, it transforms from an indirect to a direct gap semiconductor, enabling strong exciton PL at room temperature due to the direct electron transition without the loss of momentum [98]. The enhanced PL from TMDCs has been further explored to realize coherent light sources from a TMDC monolayer [15, 99–101]. In quantum-electrodynamics, local density of photonic states of exciton recombination can be modified by the environmental electromagnetic field. Plasmon–exciton coupling can be used to enhance the emission efficiencies of light-emitting materials and devices. In the surface plasmon resonant energy, the excitonic electromagnetic decay rates are dramatically enhanced, leading to improved quantum yield of PL [61]. Enhanced PL up to 12 times has been observed from the fact that plasmonic resonance couples to both excitation and emission fields and thus boosting the light–matter interaction at the nanoscale [102], see Figure 3A.

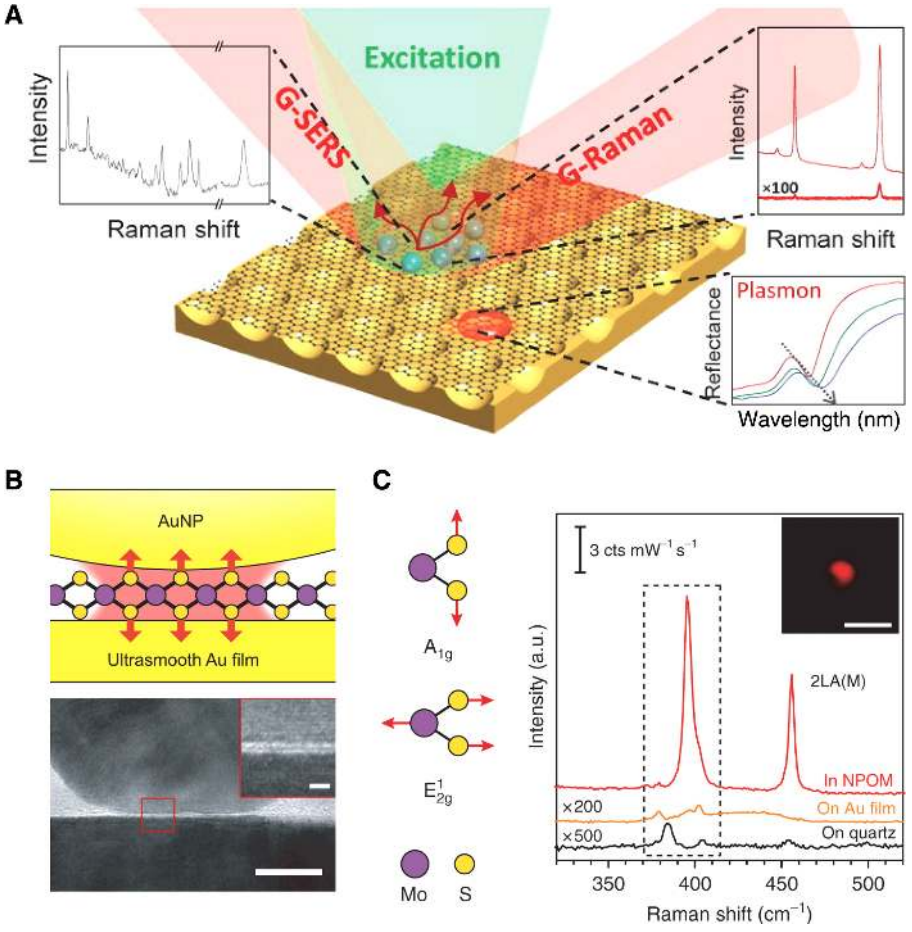

Figure 2: Raman scattering of 2D materials enhanced by plasmonic nanostructures.
(A) A hybrid graphene–plasmonic structure for studying light–matter interaction with Au-void nanostructures exhibiting resonances in the visible range. Enhanced coupling of graphene to the plasmon modes of the nanovoid arrays results in significant frequency shifts of the underlying plasmon resonances, enabling 30% enhanced absolute light absorption by adding a monolayer graphene and up to 700-fold enhancement of the Raman response of the graphene. (B) The quantitative probing of the vertical and horizontal SERS of MoS_2 inside plasmonic antennas with a gap distance reaching down to a well-defined subnanometer scale. Layered 2D MoS_2 crystals with strict lattice arrangement were designed as probes to create robust and uniform gaps with intervals of 0.62 nm, indicated by schematic and high-resolution transmission electron microscope images. (C) Atomic displacements of the phonon modes in the unit cell of 1 L MoS_2. The Raman scattering spectra and image (inset) show the plasmon-enhanced Raman signals, scale bar, 2 μm. Reproduced/adapted with permission from Zhu et al. [88] (A) and Chen et al. [92] (B, C).

In most monolayer TMDCs, the broken inversion symmetry combined with time-reversal symmetry causes opposite electron spins at the energy-momentum dispersion, so-called valleys [105, 106]. The emergence of 2D TMDCs materials has sparked intense activity in so-called valleytronics, as their valley information can be encoded and detected with the spin angular momentum of light. The valley-dependent directional coupling of light was demonstrated using a plasmonic nanowire–WS_2 system, where the valley pseudospin in WS_2 couples to transverse optical spin of the same handedness with a directional coupling efficiency of 90% ± 1% (Figure 3B) [103].

In addition, optical metasurfaces [107] can facilitate valley transport and establish an interface between valleytronic and photonic devices [108]. Specifically, plasmonic metasurfaces can evanescently interact with excitons in 2D TMDCs in the near field and at the same time apply a spin-related geometric phase to light via spatially distributed plasmonic nanoresonators. It was reported that valley-polarized PL of MoS_2 can be tailored through near-field interaction with plasmonic chiral metasurface. The resonant field of the chiral metasurface couples with valley-polarized excitons and tailors the measured PL spectra in the far field (Figure 3C and D) [104]. These plasmon-enhanced excitons are promising for application as low-power, ultrafast lasers and modulators and for the study of many-body quantum phenomena [16].

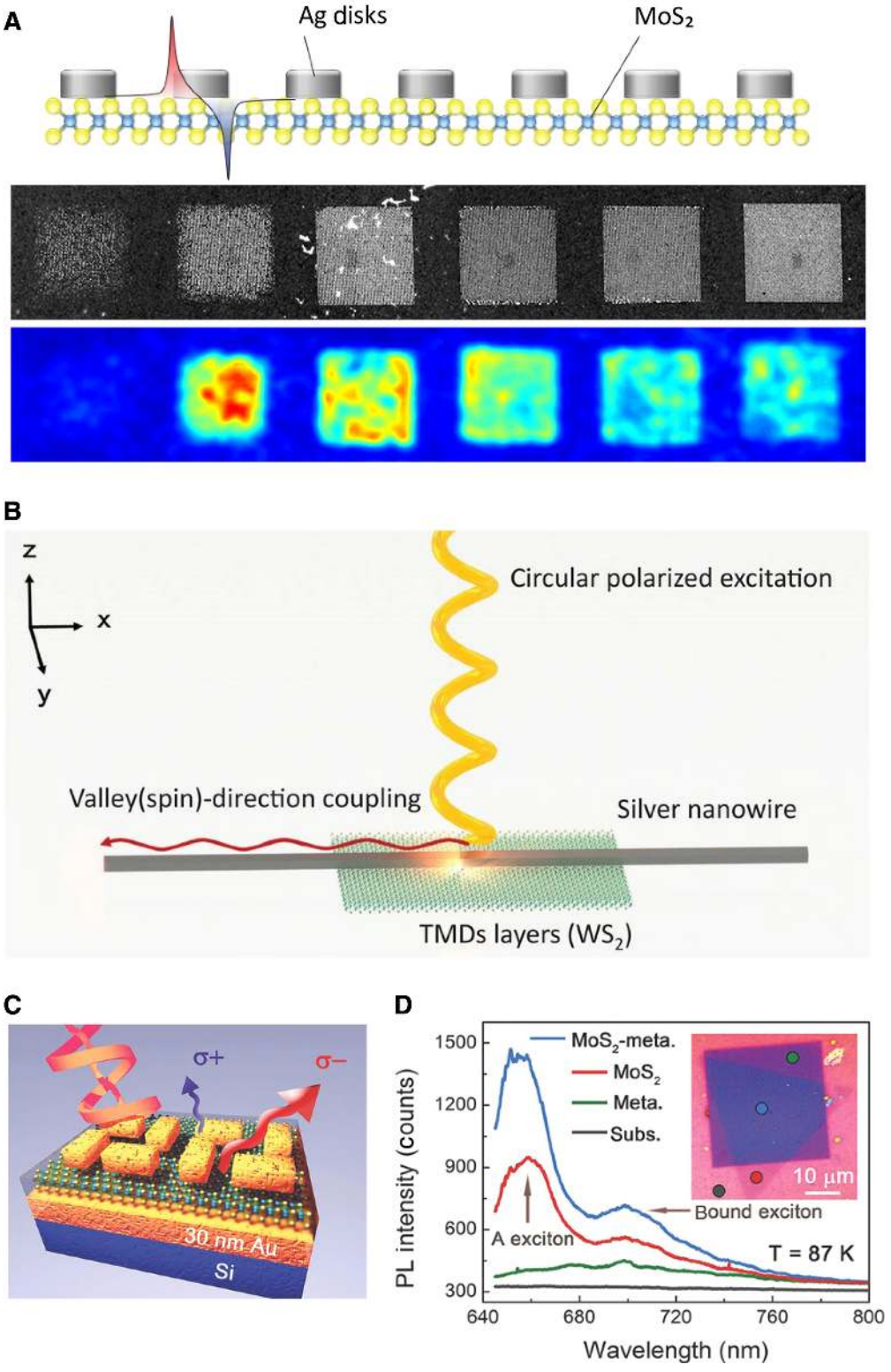

Figure 3: Enhancing PL of 2D materials by plasmonic nanostructures.
(A) Enhanced light emission from large-area monolayer MoS_2 using plasmonic silver nanodisc arrays, where enhanced PL up to 12 times was measured. (B) The valley-dependent directional coupling of light using a plasmonic nanowire–WS_2 system. It shows that the valley pseudospin in WS_2 couples to transverse optical spin of the same handedness with a directional coupling efficiency of $90 \pm 1\%$. (C) Schematic of the resonant field of the chiral metasurface coupled with valley-polarized excitons. (D) The WoS_2 metacoupling tailors the measured PL spectra in the far field at $T = 87$ K where the PL intensity of MoS_2 monolayer is enhanced by the chiral metasurface, see the inset optical image. Reproduced/adapted with permission from Butun et al. [102] (A), Gong et al. [103] (B), and Li et al. [104] (C, D).

2.3 Nonlinearity enhancement in 2D materials by plasmonic nanostructures

Nonlinear optical processes, including saturable absorption, second-harmonic generation (SHG), third-harmonic generation (THG), and two-photon absorption, enable technology for a large range of applications from light generation, quantum photonics, and attoscience to bioimaging and sensing. Two-dimensional materials also exhibit extraordinary NLO properties, which start with the case of ultrafast and broadband saturable absorption response of graphene in mode-locked lasers [109, 110].

The optical response of a material to an applied optical field can be expressed by expanding the polarization $\mathbf{P}(t)$, as a power series in terms of the optical field strength $\mathbf{E}(t)$,

$$\mathbf{P}(t) = \chi^{(1)}\mathbf{E}(t) + \chi^{(2)}\mathbf{E}(t)^2 + \chi^{(3)}\mathbf{E}(t)^3 + \ldots, \quad (1)$$

where the coefficients $\chi^{(n)}$ are the nth-order susceptibilities of the medium, and the presence of such a term is generally referred to as an nth-order nonlinearity, representing both the polarization-dependent nature of the parametric interaction and the symmetries (or lack of) of the material.

The NLO effect is sensitive both to the phase-matching condition and the crystal symmetric. Provided by the in-plain coupling from plasmonic nanostructures, a phase-matching condition is in principle satisfied for 2D materials when both the momentum and energy are conserved simultaneously. The odd-order nonlinearity, such as THG, can be observed in any symmetry, whereas all the even-order susceptibility will be vanished in the centrosymmetric material. As mentioned, 2D materials usually have very short light interaction lengths with the pump laser because they are atomically thin, such that light-harmonic generation is generally inefficient. For TMDCs, the lack of inversion symmetry at the surface can give rise to strong SHG signal under intense optical pump and plasmonic enhancement. Using remotely excited SPPs, axial collimated but transversely divergent SHG in a single silver nanowire–monolayer MoS_2 hybrid system was demonstrated to generate and manipulate SHG emission around subwavelength waveguides, as shown in Figure 4A [59]. In the work done by Wang et al. [111], a 7000-fold SHG enhancement without peak broadening or background in the spectra, was reported (Figure 4B). In addition, SHG amplitude can be dynamically controlled via selective excitation of the lateral gap plasmon by rotating the laser polarization, as shown in the right panel of Figure 4B.

Plasmonic metasurface can entangle the phase and spin of light and simultaneously enhance and manipulate nonlinear emission of the on-top 2D materials. The second-harmonic valley photons in monolayer WS_2 at room temperature were coherently pumped by light, separated, and routed to predetermined directions with a spin-related geometric phase Au metasurface (Figure 4C) [112]. The nonlinear hybrid graphene-covered plasmonic grating was proposed to realize efficient third-order nonlinear terahertz (THz) effects with a limited fabrication complexity (Figure 4D) [113]. These hybrid graphene–plasmonic structures and devices are expected to be useful for nonlinear spectroscopy, noninvasive subwavelength bioimaging, and ultrafast communication applications.

2.4 Ultrastrong light–matter interactions enabled by acoustic plasmons

As mentioned above, the light–matter interaction in 2D materials can be greatly enhanced by polaritons, taking the benefits of their extraordinary field confinement. Relying on the hybridization mechanism, plasmon polaritons with extremely large wavevectors can be achieved when the separation between two layers is decreased. Here we review recent progress of ultraconfined acoustic plasmons existing in hybrid 2D-dielectric-metal systems, particularly focusing on the investigation of the nonlocal response and quantum features of plasmons in 2D materials. As an example, acoustic graphene plasmons (AGPs) exhibiting a linear dispersion [114–116] are found in a graphene monolayer lying at a small distance d from a metal substrate, (see the top left in Figure 5A). Figure 5A shows plasmon velocity v_p and dispersion curves of AGPs as a function of the thickness d of the dielectric. The solid and dashed lines represent the results obtained by the Drude mode (so-called the local model) and random phase approximation (RPA, i.e. the nonlocal theory), respectively. One can see that the plasmon velocity becomes smaller, and the dispersion curve of the AGPs moves toward larger wavevectors as d is reduced. The classical results obtained by the Drude model agree quite well with those obtained by the RPA model for a large distance, while showing significant quantitative deviations when d is below 10 nm. Especially when the dielectric separation is on the order of a few nanometers, the classical theory totally breaks down, showing that the dispersion diagram falls within the electron–hole continuum and that the plasmon velocities are below the Fermi velocity of carriers in graphene, which are prohibited by the nonlocal theory. The strongly confined AGP supported in the system consisting of hexagonal

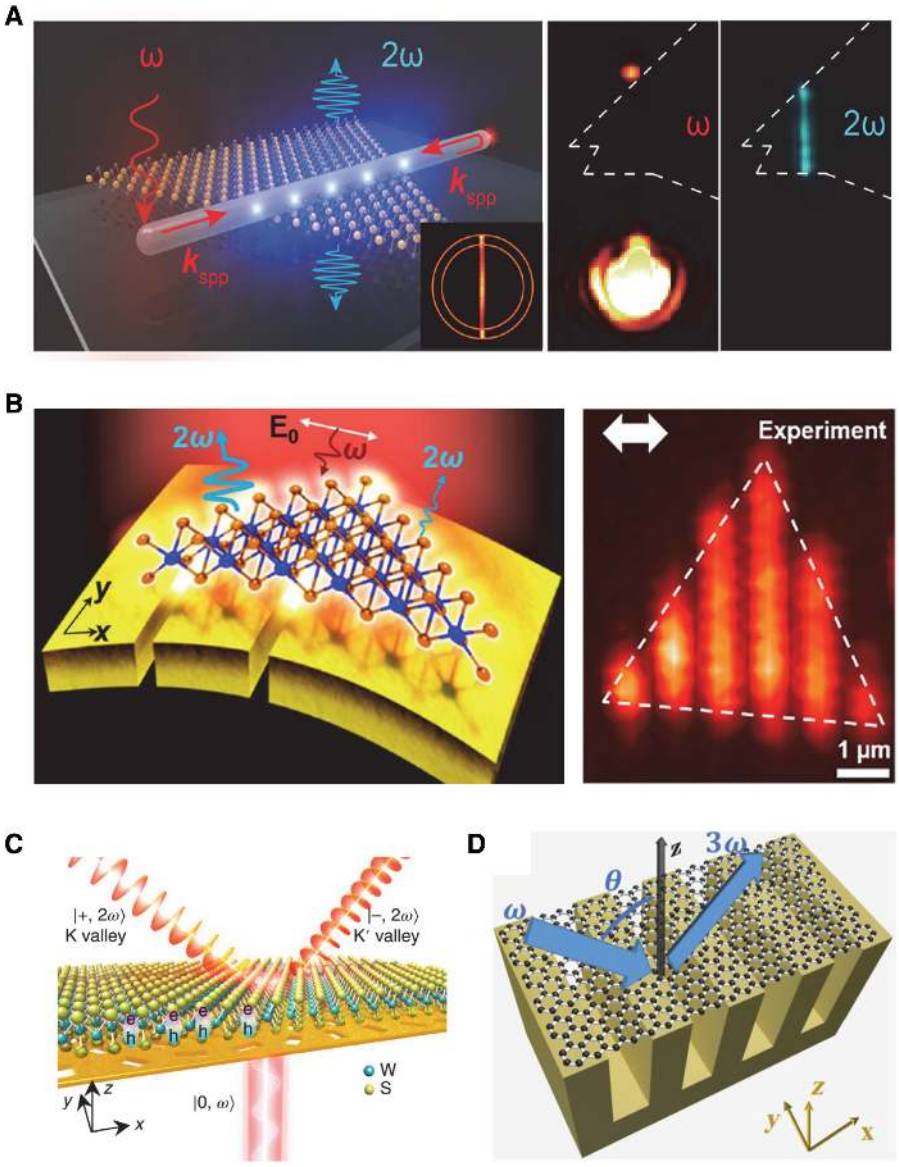

Figure 4: Nonlinearity enhancement in 2D materials by plasmonic nanostructures.
(A) Left, SHG from silver nanowire–monolayer MoS_2 hybrid structure; Middle, Optical imaging under the excitation wavelength of 796 nm; right, imaging at SH frequency, the white dotted line is the outline of monolayer MoS_2. (B) Left, SHG from monolayer WSe_2 on the Au trench hybrid system; right, enhanced SHG mapping at the transverse polarization resonant excitation. The white dotted line is the outline of monolayer WSe_2. (C) A synthetic structure with a plasmonic metasurface substrate can yield large SHG from the valley band of the WS_2 and split opposite spin components of the second-harmonic valley photons into different directions. (D) A proposed hybrid graphene–plasmonic grating to achieve enhanced nonlinear effects at terahertz frequencies. Reproduced/adapted with permission from Li et al. [59] (A), Wang et al. [111] (B), Hu et al. [112] (C), and Guo et al. [113] (D).

boron nitride (hBN)–encapsulated graphene deposited onto a metal gate [117] was first experimentally visualized [117] by scattering-type scanning near-field optical microscope (s-SNOM) [120, 121]. A nanoscale-resolved THz photocurrent near-field microscopy was developed (see the top left in Figure 5B), where the near-field AGPs were detected thermoelectrically [122]. The near-field photocurrent (see the bottom-left in Figure 5B), in the graphene was measured by the two metal contacts. By measuring the oscillation period for the photocurrent profiles as a function of frequency, the dispersion relation for the AGPs was experimentally obtained (see the red symbols in the right panel in Figure 5B, showing a nearly linear dispersion at low frequencies). The experimental results were found to be consistent with calculated dispersion (see the blue contour plot in the right panel).

Due to the linear dispersion, AGPs have the potential to achieve extremely large wavevectors, while having their

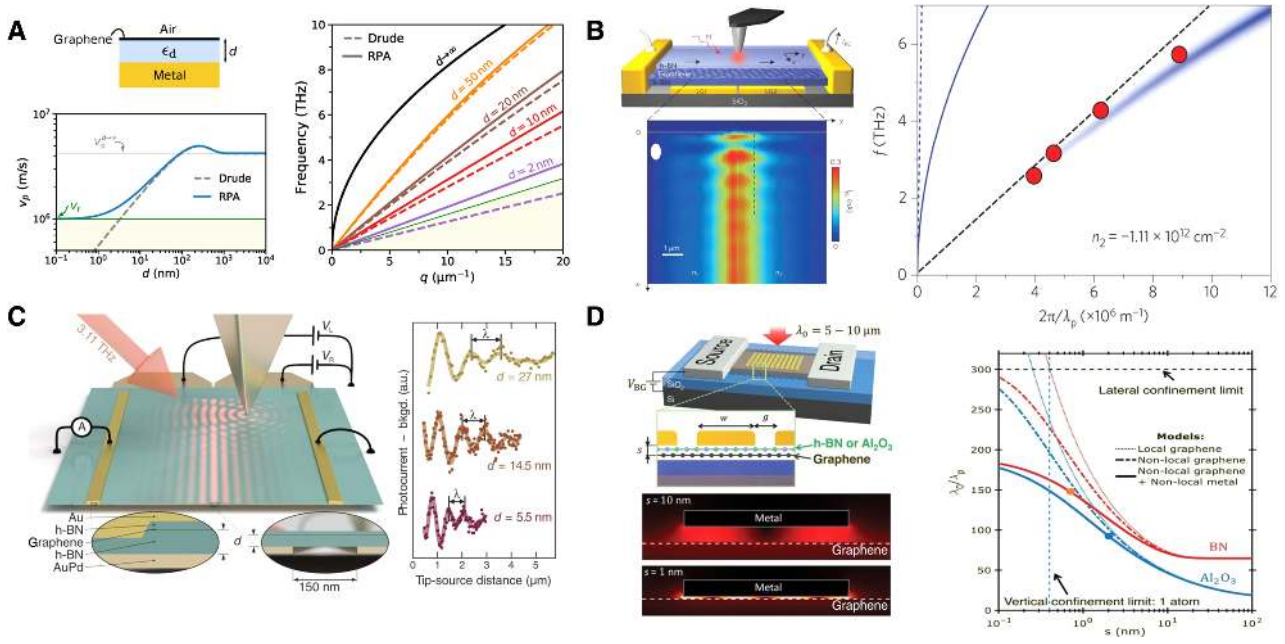

Figure 5: Ultrastrong light–matter interactions enabled by acoustic plasmons.
(A) Plasmon velocity v_p and dispersion curves of acoustic graphene plasmons supported by a graphene-dielectric-metal system as a function of the thickness d of the dielectric separating a graphene layer from a metal substrate. Both the local and nonlocal responses for AGP are considered, whereas the metal is assumed to be a perfect electric conductor. (B) Left, Schematics of the experimental setup and real-space imaging of acoustic graphene plasmons in a graphene photodetector with split-gate architecture, where the laser-illuminated metal tip of an atomic force microscope serves as a nanoscale near-field light source. Right, The dispersion of AGPs obtained by s-SNOM, see the red symbols, showing a nearly linear dispersion at low frequencies. (C) Left, Schematics of the experimental setup, where terahertz laser illuminates the device, launching the AGP. Right, Photocurrent profiles for three different devices and their corresponding plasmon wavelength λ. (D) Left, Device design for probing ultimate confinement limit for AGP and simulated plasmonic fields for the separations at 10 and 1 nm. Right, Simulated plasmon wavelength as a function of metal–graphene separation under four different models. Reproduced/adapted with permission from Gonçalves et al. [57] (A), Alonso-González et al. [117] (B), Lundeberg et al. [118] (C), and Alcaraz Iranzo et al. [119] (D).

associated plasmon velocity close to the Fermi velocity of carriers in graphene when the graphene–metal separation is largely reduced. In principle, the distance between the graphene and metal can amount to the single-atom thickness if we choose a single-layer of hBN as a spacer. Therefore, the unique 2D-dielectric-metal system allows us to study nonlocal effects and to probe the quantum mechanical features [118, 123, 124]), as discussed in Figure 5A. Lundeberg et al. [118] investigated experimentally the nonlocal response of graphene electron liquid. Notably, Figure 5A shows the concept for enhancing nonlocal effects by slowing down the velocity of graphene plasmons. The left panel of Figure 5C shows the experimental setup, where the graphene is encapsulated by hBN [125] and placed on the top of AuPd metal layer. Three devices with different graphene–metal separation were fabricated and were all electrically contacted by use of one-dimensional electrical contact to the 2D material [126]. The s-SNOM in the photocurrent mode was used to visualize and characterize AGPs. The measured photocurrent profiles (see the right panel in Figure 5C) shows the interference fringes in the dependence of tip position, allowing us to determine the plasmon wavelength λ by fitting to the photocurrent with an appropriately subtracted background. The plasmon phase velocity was extracted from the photocurrent maps for three devices, and it turned out that the local approximation showed a significant discrepancy, while showing excellent agreement for the full nonlocal theory.

The hybrid 2D-dielectric-metal structure provides a unique platform to probe the ultimate plasmon confinement limits. Alcaraz Iranzo et al. [119] fabricated the 2D-dielectric-metal heterostructure consisting of monolayer of graphene and an array of metallic rods, separated by hBN or Al_2O_3 (see the top left in Figure 5D). Here the presence of the metallic rods leads to efficient screening of graphene plasmons, at the same time facilitating efficient coupling between far-field light and the strongly confined AGPs. The field profiles shown in the left-down in Figure 5D illustrate the strong field confinement between the metal and graphene. Bringing the metal closer to the graphene layer significantly enhances the vertical confinement (see the right panel in Figure 5D), where the simulated results

were obtained under four different models. These ultraconfined plasmon modes, discussed in [118, 119, 124], give rise to realize ultrastrong light–matter interactions.

3 Plasmon-enhanced photonic devices based on 2D materials

In the recent decades, we have witnessed an explosive increase in the data traffic owing to the internet era [127, 128]. Owing to its superior advantages, such as low loss, high speed, and low cost, optical communication technology plays a vital role in nearly every aspect of the modern communication systems, such as access, aggregation, and core networks [129–131]. Since the pioneer demonstrations of integrated optical interconnects, such as on-chip lasers [132, 133], modulators [134], and photodetectors [135, 136], remarkable progress has been made in achieving better performance of these devices by using various materials with distinctive optoelectronic properties [137]. Two main material categories are Si and III/V materials. Silicon technology is mainly utilized in optical filters [138–140], switches [141–143], delay lines [144–146], and modulators [147–151], thanks to its low propagation loss. On the other hand, III/V materials have been widely applied to on-chip lasers [152, 153] and photodetectors [154, 155], due to their direct bandgap. The emerging of novel technology, such as the 5G net [156], high-performance computing [157], and artificial intelligence [158], has driven the industry evolution with an even higher demand for the data communication capacity in the future. To meet such demands, the integrated devices forming optical interconnects need to support large-scale bandwidth operation and with ultralow-power consumption, while maintaining its scalability and low-cost manufacturing. Unfortunately, these demands could hardly be fully satisfied by laying on the existing bulk material systems.

Because of ultrahigh carrier mobility larger than 200,000 $cm^2 V^{-1} s^{-1}$ [159–163], 2D materials have been recognized as ideal supplements toward the bulk materials in realizing ultrahigh-speed operation with ultralow-power consumption. However, when integrated with conventional devices, the atomic-scale-thickness 2D materials could significantly hinder the device's performance due to its inherently weak light–matter interaction. Significant efforts have been devoted to enhance the light–matter interaction, such as employing microcavities [164, 165], slow-light photonic devices [166, 167], or double-layer 2D materials [37, 168]. Besides these well-known methods, SPPs are also widely applied with 2D materials to enhance the light–matter interaction and to achieve high-performance photonic devices, thanks to their subwavelength light confinement ability and significant field-enhancing effect. This subwavelength light confinement of the plasmonic devices could be highly valuable toward the high-density integration for the optical interconnects in the future [77–80]. In this section, we review plasmon-enhanced photonic devices based on 2D materials. Two key building blocks for the optical interconnects, that is, modulators and photodetectors, are to be addressed. Other devices based on 2D materials and plasmonic nanostructures are discussed in the perspective and conclusion section.

3.1 Hybrid 2D material plasmonic modulators

Being a crucial component in the optical interconnects, electro-optic modulators convert the electrical signal into optical signal in order to take advantage of the high speed and low power consumption in the optical domain. Multiple attributes of light can be employed to achieve light modulation, including amplitude, phase, and polarization [147, 169, 170]. Up to now, most of high-speed integrated electro-optical modulators, especially Si modulators, heavily rely on the plasma dispersion effect [171]. The plasma dispersion effect is related to change the density of free carriers in a semiconductor. Other effects, such as thermo-optic effect [172], Franz–Keldysh effect [173], quantum-confined Stark effect [174], and Kerr effect [175], could also be used for the optical modulators. The key figures of merit used to characterize a modulator are the speed, modulation depth, and operation wavelength range. Although impressive progress has been made in the integrated electro-optic modulators, many reported modulators based on the bulk material still face crucial challenges in realizing ultrahigh-speed modulation, owing to their relatively low carrier mobility.

Because of ultrahigh carrier mobility in 2D materials, they could provide the possibility to realize ultrahigh-speed modulation when combined with conventional optoelectronic devices [176]. Among them, graphene has been extensively explored for the application in electro-optic modulator. Most of graphene-based modulators rely on gate-tunable electroabsorption effect, thus acting as an intensity modulator [32, 177, 178]. It could also perform as a phase modulator by applying a Mach–Zehnder interferometer configuration [179, 180]. The most distinctive performance of the reported graphene modulators lies in its potential to realize extremely high modulation speed. For instance, the all-optical modulator reported by Li et al. shows a response time of 2.2 ps, which is equivalent to a

calculated bandwidth of 200 GHz [178]. Another significant advantage originating from the gapless nature of graphene is its broad operation bandwidth, which has been demonstrated to cover visible, infrared, and THz bands [181]. However, for these Si-based 2D material modulators, the optical modes are usually strongly confined in the high-index materials, leading to weak light–matter interaction, as well as poor modulation depth. Besides, the size of the reported modulators is normally limited in tens of microns in order to reach the designed moderate modulation depth [182], which may further impede the miniaturization of the devices.

Because SPPs show the ability to manipulate light on the subwavelength scale, it could be used to direct more energy of light into a 2D material to enhance the performance for a 2D-based device, as well as to shrink the size of a 2D-based modulator. Extensive researches have been conducted to demonstrate graphene-based modulators by taking advantage of the plasmonic nanostructures. Early works were devoted in the flexible control of plasmon excitation [183, 184], plasmon resonance wavelength [185, 186], or plasmon resonance quality factor [187]. Various metallic nanostructures, including Au nanorod, Au strip, Au bowties, and Ag nanowires, were introduced to stimulate plasmonic modes. Although graphene is only a single-atom thick, its effect on altering the plasmonic wave is remarkably strong. For example, in a hybrid graphene–Au nanorod system proposed by Kim et al. [185], a 20-meV shift of resonance frequency, 30% increase in quality factor, and resonance scattering intensity were experimentally observed by applying different gate voltage, as shown in the Figure 6A. Moreover,

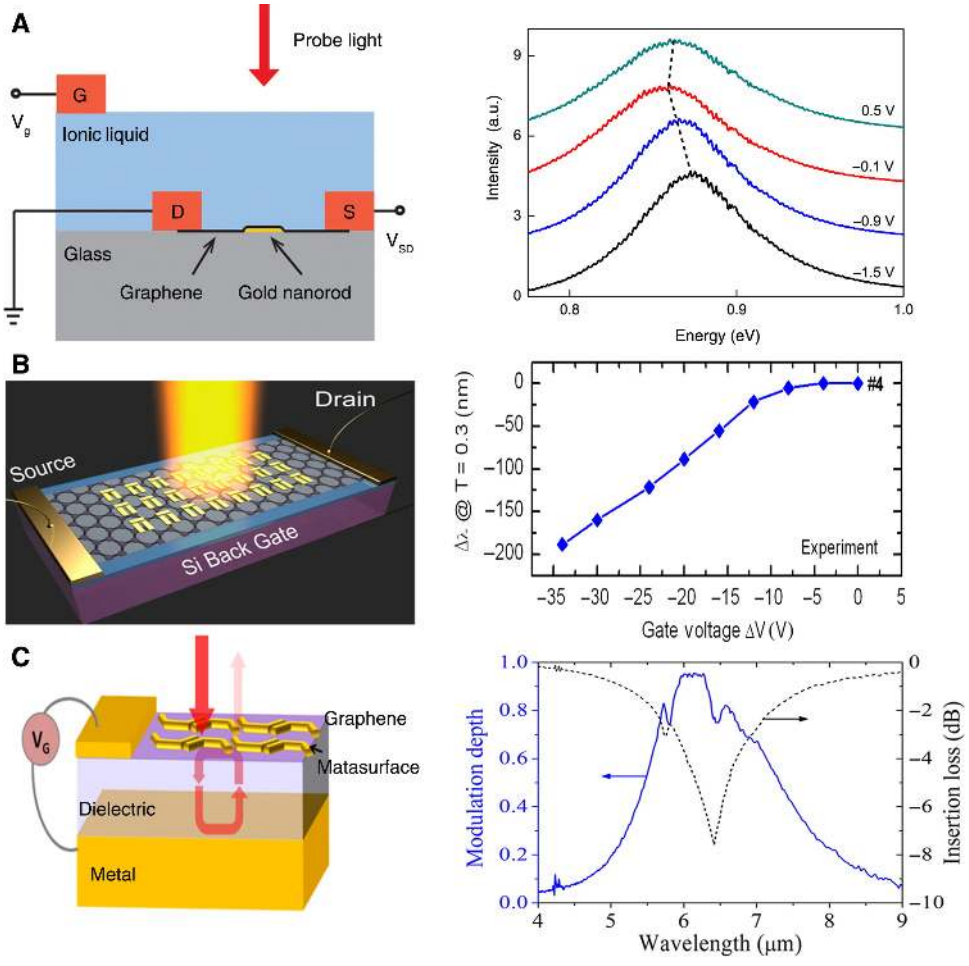

Figure 6: Plasmonically enhanced electro-optic modulation under normal illumination.
(A) The hybrid graphene–Au nanorod system exhibits a 20-meV shift of resonance frequency and a 30% increase in quality factor upon external voltage. (B) Metallic bowties are employed to enhanced light–matter interaction within the channel region of FET, resulting in an effective modulation with a resonance wavelength decrease of 210 nm. (C) Metallic nanostructures are placed on top of the graphene, which combine with the metal reflector on the bottom of the dielectric interlayer. The designed structure forms a perfect absorber, exhibiting a modulation depth up to 100%. Reproduced/adapted with permission from Kim et al. [185] (A), Emani et al. [187] (B), and Yao et al. [188] (C).

by combining the graphene sheet with metallic bowties, Emani et al. [187] demonstrated that the transmittance of infrared incident light could also be effectively modulated by changing the gating of graphene, which is displayed in Figure 6B. The decrease in resonance linewidth was experimentally observed to be up to 210 nm by applying external voltage of 35 V. The metallic nanostructure, as a metasurface, could also be utilized to demonstrate perfect absorbing with the aid of the metallic mirror, which is shown in Figure 6C. By switching the absorber in and out of the critical coupling condition via the gate voltage applied on graphene, an impressive modulation depth up to 100% was achieved [188], which could hardly be realized only with graphene. Meanwhile, they also demonstrated a modulation bandwidth up to 20 GHz over a broad wavelength range. Although these early works rely on top illumination and operate within infrared wavelength, which might not be readily applied for the optical interconnects, they could be recognized as endeavor, demonstrating the feasibility for the plasmonic graphene modulator.

Compared to the device with top illumination, waveguide-type modulators are much more favorable due to the compatibility with other devices in terms of the large-scale photonic integration. By taking the benefits of SPPs, plasmonically enhanced waveguide-type modulators have attracted more and more attention in recent years. The hybrid graphene–plasmonic waveguide modulator was first demonstrated by Ansell et al. [189]. In their design, the gold strip supporting SPPs is covered by an hBN, which acts as a dielectric spacer. Three different plasmonic modes, that is, flat plasmons (FPs), corrugated plasmons (CPs), and wedge plasmons (WPs), can be excited separately by focusing the incident light beam with the wavelength of 1.5 μm to different parts of the coupler, as illustrated in Figure 7A. The modulation was achieved by applying gating to the graphene sheet, thus

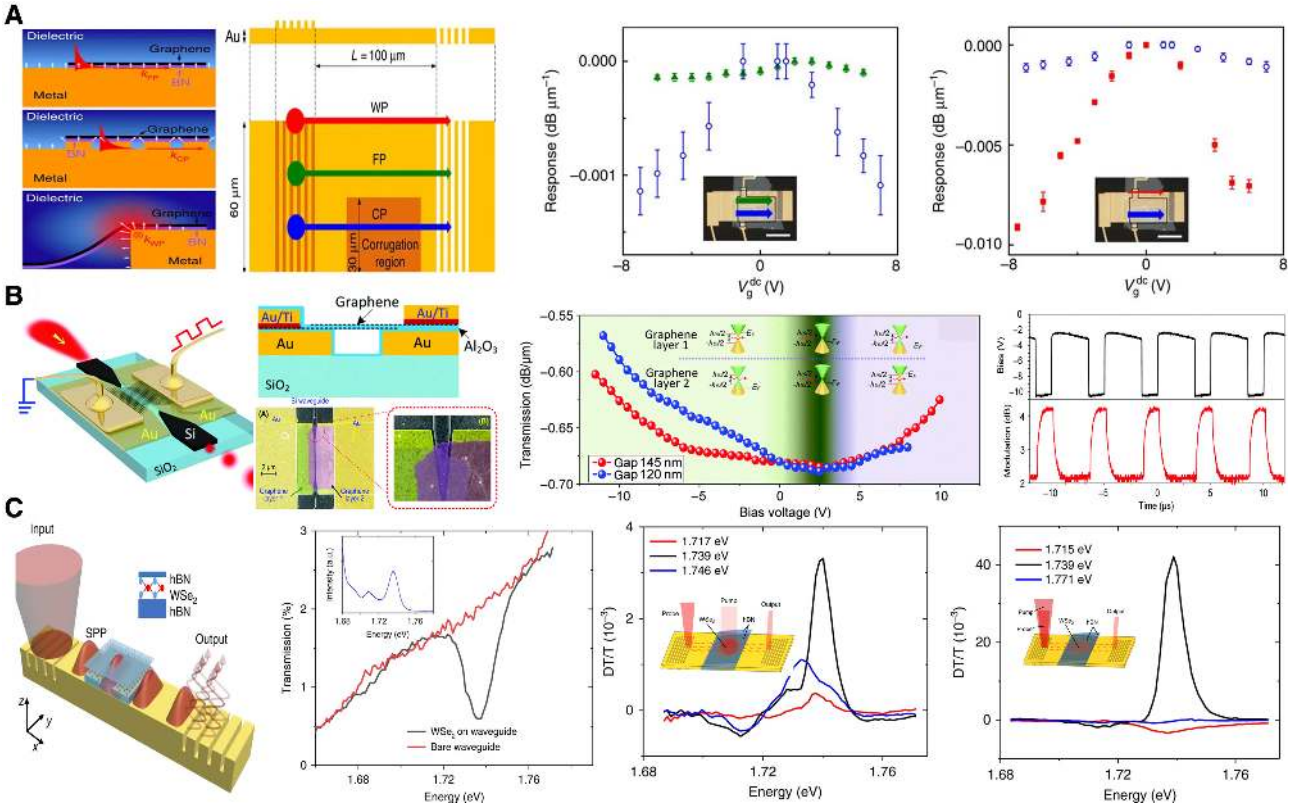

Figure 7: Plasmonic waveguide optical modulators.
(A) Three different SPP modes supported by different structures, which are flat plasmons, corrugated plasmons, and wedge plasmons, respectively. The highest modulation depth of 0.03 dB/μm is reached for the wedge plasmons. (B) An efficient modulator based on the leaky mode of plasmonic slot waveguides. The leaky mode is achieved by optimization of the hybrid waveguide to ensure a low insertion loss of 0.68 dB/μm. The modulation depth is 0.13 dB/μm, and modulation bandwidth is 200 kHz. (C) Plasmonic modulator based on monolayer WSe_2 encapsulated by hBN. The SPP is excited either by the metallic grating or by the metallic surface. The modulation could be realized by either plasmonic control or optical control, which has a modulation depth of 0.004 dB/μm and 0.04 dB/μm, respectively. Reproduced/adapted with permission from Ansell et al. [189] (A), Ding et al. [34] (B), and Klein et al. [190] (C).

changing the light absorption rate within the waveguide. Among these three modes, WPs exhibited highest modulation depth of 0.03 dB/μm, which is 30 and 230 times larger than the performance of CPs and FPs modes, thanks to its strong interaction with graphene. Although the proposed modulator might not hold best modulation performance, it paves a promising way toward practical realization of very compact and efficient, potentially ultrafast, and broadband hybrid graphene–plasmonic optical modulator at 1550 nm.

In order to improve the modulation depth, Ding et al. [34] proposed an efficient modulator based on leaky-mode plasmonic slot waveguides. The plasmonic slot waveguide (Figure 7B) was formed by introducing a small slot in a thin Au sheet. Two layers of graphene with a thin layer of Al2O3 form an effective capacitor, thus enabling modulation of the light propagation in the waveguide through tuning the optical absorption of graphene sheet. They experimentally demonstrated the modulation depth of 0.13 dB/μm with relatively low propagation loss of 0.68 dB/μm for the slot width of 120 nm. More importantly, the demonstrated modulator was fully integrated with Si technology, where the light was coupled in/out the plasmonic waveguide by use of a tapered Si waveguide. The high modulation depth corresponds to a considerable extinction ration of 2.1 dB in the dynamic performance characterization. Although the modulation bandwidth is approximately only 200 kHz, which is limited by the large RC constant of the device, the proposed device holds the highest modulation depth of the graphene modulator based on plasmonic waveguides. Further optimization of the response time can be achieved by using optimized structure, such as metal–insulator–metal waveguide, which has an ultrafast response time of 2.2 ps.

Besides graphene, TMDCs also exhibit impressive optoelectronic properties including large third-order NLO susceptibilities and strong light–matter interaction [191, 192]. Most recently, Klein et al. [190] proposed a plasmonic modulator based on WSe2 monolayer integrated on top of a metallic waveguide. As shown in Figure 7C, WSe2 monolayer is electrically isolated from the metal by encapsulating with hBN. Two different methods to control the SPP propagation were experimentally demonstrated in their work, which were optical control and plasmonic control, respectively. The modulation was realized by the strong interaction between the SPPs and excitons in the WSe2 monolayer. In both schemes, the SPPs were excited by focusing the light onto the metal grating coupler. For light control scheme, another free-space laser was focused on the hBN-WSe2-hBN structure to act as optical pump. The modulator had a normalized transmission change of 4.1×10^{-3} with the pump energy of 1.739 eV, equivalent to a modulation depth of 0.004 dB/μm. For the plasmonic control, however, both the pump and probe laser were coupled into the input grating coupler. The normalized transmission change is 10-fold larger than that of the optical pump scheme, which reaches 4.1×10^{-2} with the pump energy of 1.739 eV. This value corresponds to a modulation depth of 0.004 dB/μm. Moreover, the response time was experimentally verified to be 290 fs, equivalent to a modulation bandwidth of 1.5 THz. The performance of this plasmonic modulator with 2D material is quite impressive, including high modulation depth of 73% and fast response time comparable to the previously reported plasmonic modulator [34], as well as ultralow power consumption of 650 fJ pump energy. Although these performances were achieved under low temperature (around 10 K) in order to prevent thermal broadening effect, it still could be recognized as a milestone in the area of the plasmonic modulator based on the 2D material. As another important member in the 2D materials family, black phosphorus (BP) and its analog have also been utilized in realizing optical modulation, as well as the Q-switched laser [193–197]. One of the representative works was reported by Peng et al. in 2018 [198]. When the BP is integrated with Si waveguide, a 5-dB modulation depth and 1-dB insertion loss could be expected based on the measured results of absorption coefficient. However, the integration of BP and metallic nanostructures is yet to be investigated up to now.

3.2 Hybrid 2D materials plasmonic photodetectors

As an opposite building block of optical modulator, photodetectors can convert the light signal into the electrical signal for the subsequent processing. Several bulk materials have been widely used in the integrated photodetectors, such as Si [199–202], germanium (Ge) [203–208], and III/V materials [209–211]. To date, most commercialized integrated photodetectors for optical communication wavelength are based on III/V materials. However, they hold several disadvantages impeding its practical applications including high cost and incompatibility with the compatible metal-oxide semiconductor (CMOS) technology. For example, Ge is an appealing absorbing material for optical communication wavelength and has been widely investigated. However, the large dark current and limited operation bandwidth requires to be addressed before its practical application. Silicon-based photonic components are especially attractive for realizing low-cost photonic integrated circuits using high-volume

manufacturing processes, thanks to its high compatibility with the mature CMOS industry. Due to its transparency in the telecommunications wavelength bands near 1310 and 1550 nm, Si is an excellent material for realizing low-loss passive optical components [212]. For the same reason, however, it is not a strong candidate for detectors, which requires material to have strong light absorption. Therefore, most integrated photodetectors employ either III/V materials or Ge as absorption medium. Although impressive performance based on these two material systems has been demonstrated, both of them hold distinct drawbacks including the incompatibility with Si photonics and large dark current and difficulty in reaching high responsivity and large operation bandwidth simultaneously. Thanks to its gapless nature, graphene exhibits a wavelength-independent absorption property, ranging from ultraviolet to THz regime. Moreover, graphene also holds great potential in reaching ultrahigh operation bandwidth. Based on all these reasons mentioned above, graphene has been widely explored for the photodetector integrated with plasmonic devices, in order to reach high-speed photodetection.

The first generation of the plasmonic photodetector with 2D materials is based on the free-space scheme, which directly projects light onto the absorption region. Among them, Xia et al. [213] proposed one of the earliest graphene photodetectors. In their work, although plasmonic structures are not directly utilized to increase the light absorption, the enhancement near the metal–graphene interface was observed. In 2011, Echtermeyer et al. [77] increased the responsivity of the photodetector by up to 20 times, thanks to the combination of graphene and plasmonic nanostructures. Various types of nanostructures were fabricated and investigated, and they found that the grating with 110-nm finger-width and 300-nm pitch showed the best performance, where the scanning electron microscope image of the structure is shown in Figure 8A. The photovoltage mapping shown in Figure 8A exhibits clear responsivity enhancement near the tips of the nanostructures, which could be ascribed to both large electron band bending and the strong enhancement of the optical field caused by the plasmonic effect. Among all the different polarization states and excitation wavelengths for normal light incidence, the maximum enhancement was observed at 514 nm with a transverse polarization. Similar conceptual demonstration was also reported in nanogap, nanoparticles, or nanoscale antennas. Unlike other structures, Fang et al. [214] proposed a novel graphene-based structure by sandwiching nanoscale antennas between two graphene monolayers (Figure 8B). Each nanoantenna is formed by an Au heptamer with seven individual components with diameter of 130 nm and gap distance of 15 nm. The main physical mechanism of the light absorption enhancement is ascribed to the excitation of tunable Fano resonances. It strongly suppresses the scattering near-transparency window and contributes to hot electron–hole pair generation, thus enhancing the direct excitation of electron–hole pairs in a single-atom-thick graphene layer and leading to higher photocurrent. The photoresponsivity of 13 mA/W was experimentally obtained, and the photocurrent also increased when having larger heptamer sizes. Compared to the structure without antennas, an 800% enhancement of the photocurrent was observed. Although the maximum photoresponsivity remains low, approximately only 10 mA/W, it directly proved the viability of the concept of using plasmonic nanostructures for light harvesting in 2D material–based photodetectors. Last but not least, the response time of these devices mentioned above was not studied, which is another crucial parameter of the photodetection.

One of the earliest works investigating the temporal property of 2D materials plasmonic photodetectors based on the free-space scheme was reported by Sun et al. [215] in 2017. Unlike conventional plasmonic structures that usually utilize bulk metals as nanostructures, they used self-doped colloidal copper phosphide quantum dots (QDs) both as plasmonic enhancement structure and as tunable light absorption medium. The schematic of the photodetector is displayed in Figure 8C. Except for the plasmonic enhancement effect, the copper phosphide nanocrystals could also induce strong doping in graphene, which enables the formation of a p–n junction by partially covering graphene, thus leading to efficient photodetection. They experimentally demonstrated an impressive responsivity of 105 A/W at visible wavelength (405 nm) and a high responsivity of 9.34 A/W at 1550 nm. The excellent photoresponsivity is attributed to these three aspects: strong light absorption in the copper phosphide nanocrystals, the high carrier mobility in the graphene film, and the plasmon-enhanced NLO properties. Although the hybrid system of copper phosphide and graphene exhibits very high responsivity, the measured rise and decay times of the graphene–copper phosphide hybrid photodetector are only 0.42 and 1 s, respectively. The response time is far below the requirement of today's high-speed optical network, which could severely limit the potential application of the proposed device. Similar concept of combining QDs with graphene as the photodetection medium was also proposed by Ni et al. [217], with the similar photoresponsivity performance.

Besides graphene, monolayer MoS_2 has also been widely explored as the photodetection material due to its

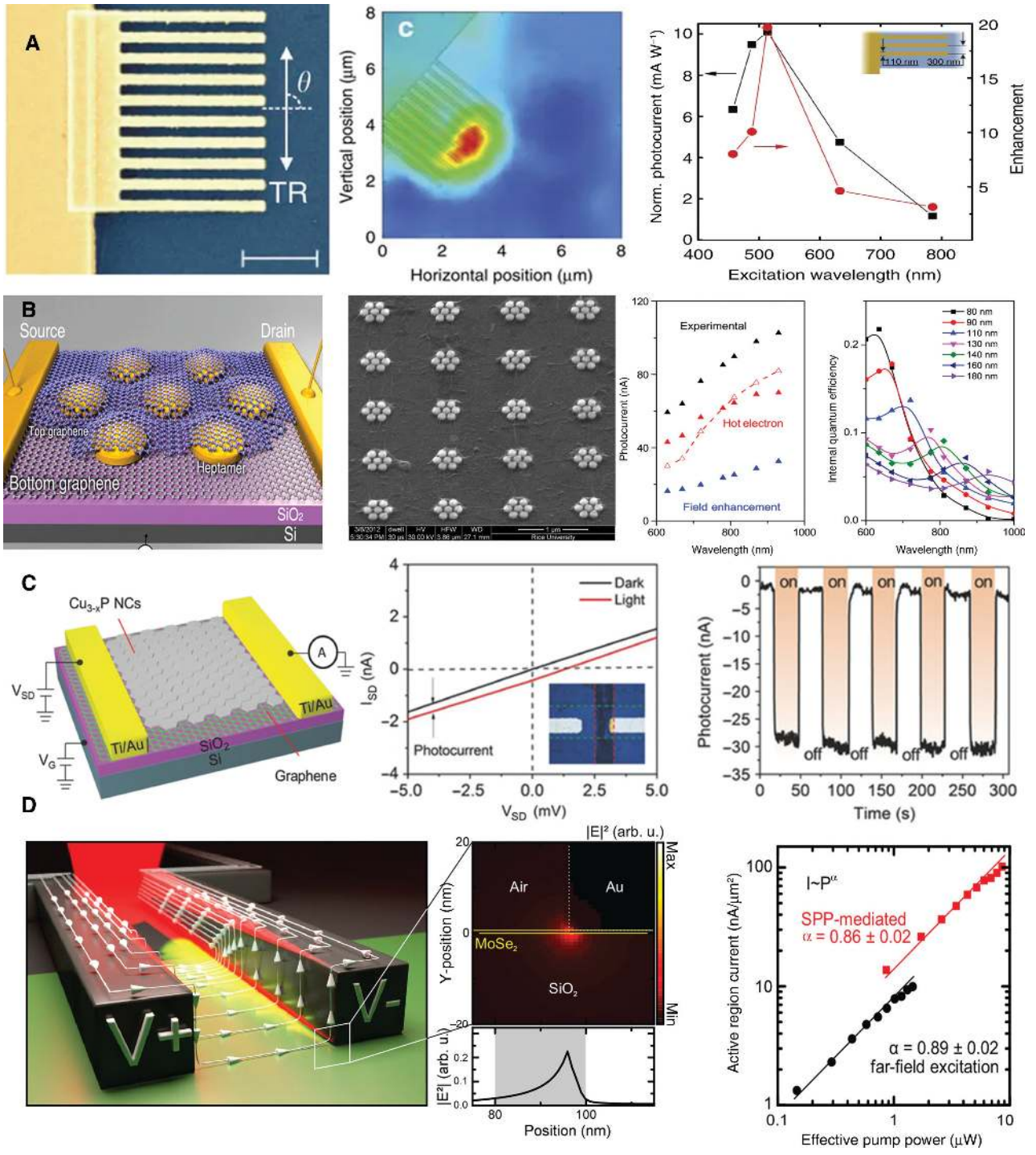

Figure 8: Two-dimensional materials plasmonic hybrid photodetectors with top illumination.
(A) Interdigit metallic strip is deposited on top of the graphene to induce plasmonic enhancement. The finger width is 110-nm finger-width, and the pitch is 300 nm. The experiment data exhibit a 20-times higher photoresponsivity compared to the device without metallic nanostructure. (B) Au heptamer is sandwiched between top layer graphene and bottom layer graphene to enhance photodetection effect. The measured data show an 800% enhancement of the photocurrent. (C) Graphene photodetector integrated with QDs. The I-V curve of the 405-nm incident light and the temporal response of 1550 nm is shown. (D) Plasmonic MoS_2 photodetector with a subwavelength size of detection region. The SPP-mediated responsivity is up to 18 mA/W, with the detection region of 0.03 μm². Reproduced/adapted with permission from Echtermeyer et al. (A), Fang et al. [214] (B), Sun et al. [215] (C), and Blauth et al. [216] (D).

direct bandgap at the visible wavelength as well as near-unity radiative internal quantum efficiency [98, 191, 218]. More recently, Blauth et al. [216] experimentally realized an ultracompact photodetector by integrating monolayer MoS_2 with a plasmonic waveguide. Figure 8D shows the schematic of the proposed device. The plasmonic waveguide was formed by two Au metallic strips, located on top of the MoS_2 layer. When the light is focused on the device, SPPs are excited and propagate toward the nanoscale detection region, which is centralized around the metal-MoS_2 interface with a subwavelength size of only 0.03 μm^2. Moreover, one can see the distinctively enhanced electrical field at the edge of the Au and MoS_2, leading to strong light–matter interactions, as well as enhanced photoresponsivity. The SPPs-mediated light absorption could yield a responsivity up to 18 mA/W. Despite that the value is not very impressive, the ultrasmall detection region demonstrated in this work could be a potential solution toward the dense on-chip integration of photonic circuit in the future.

Although plasmonic photodetectors based on free-space scheme could provide more convenience in the potential applications, they hold several intrinsic drawbacks including low responsivity and narrow bandwidth owing to large size and poor light confinement. Guiding the light into the waveguide is considered as a promising solution to boost the performance of the photodetector. Because of intrinsic loss of the metal, the metallic nanostructures may induce strong excess loss when integrated with optical waveguides. Careful designs should be taken in terms of utilizing the plasmonic enhancement effect without sacrificing the insertion losses. Therefore, both the design and the fabrication could be more complex than the case for the free-space scheme. At an early stage, researchers proposed to use the graphene strip for the waveguide and graphene ribbons for the photodetector [219]. But the insertion loss of the graphene waveguide is extremely high, thus rendering the photoresponsivity of the device. Then people started to use low-loss platform, such as Si or SiN waveguide to be integrated with the plasmonic waveguide. As one of the representative works, Ding et al. [35] reported an ultracompact graphene plasmonic photodetector on the Si platform. The schematic of the device is shown in the inset of Figure 9A. The plasmonic mode is excited by the optical mode in a tapered Si waveguide. Here the metal is considered as the material for the waveguide, as well as for the contact. The subwavelength confinement of the plasmonic mode gives rise to strong light–graphene interaction, and the narrow plasmonic slot enables short drift paths for the photogenerated carriers. In order to break the inversion symmetry, two different metals (Ti and Pd) were employed, which could induce potential difference for the contacts. The light absorption was increased by one-order of magnitude higher than the device without metal slot, reaching 1 dB/μm. By applying an external voltage of 2.2 V and increasing the length of the device to 19 μm, an impressive responsivity of 360 mA/W was experimentally reached. Another crucial benefit resulting from the narrow slot is the ultrahigh-speed photodetection. The ultrawide bandwidth larger than 110 GHz was experimentally demonstrated, confirmed by several characterization methods. The underlying mechanism could be ascribed to both the ultrafast transit of photogenerated carriers and the strong built-in electrical field within the narrow gap. Another graphene photodetector based on the metal slot was reported by Ma et al. [220] in 2019 (Figure 9B). Although the structure is to some extent similar to [35], significant differences could still be found in their work. One of the major differences is that the gap size is further reduced to only 15 nm, resulting in fundamental change of the photodetection mechanism within the device. It turned out that both photovoltaic (PV) and photobolometric (PB) played the dominant role. The highest photoresponsivity based on these two effects are 0.35 and 0.17 A/W, respectively, with the waveguide length of only 5 μm. Considering the ultracompact footprint, the photoresponsivity of the device was quite impressive. However, the bandwidth of the proposed device was not mentioned. Very recently, Muench et al. [223] reported a plasmonically enhanced graphene photodetector employing the photothermoelectric effect. The metallic slot remains to be the key structure, although the input light was converted to the voltage signal rather than current signal in PB or PV effect. Based on their measurement results, the plasmonically enhanced structure generates the external responsivity of 12.2 V/W and a 3-dB bandwidth of 42 GHz. Considering that the subsequent electrical circuit would prefer voltage signal from the photodetector rather than current signal, this design holds considerable application potential in the future, if the fabrication process could be simplified.

Besides the metallic slot structure, arrayed metallic bowtie was also utilized to improve the performance of the 2D-based photodetector [221]. As shown in Figure 9C, the light was guided by the SiN waveguide, and the nanostructured bowties were positioned on top of the graphene. The strong field enhancement arisen by the bowtie structure can be seen in the inset of the schematic. Except for the well-known plasmonically enhanced light–graphene interaction, the arrayed bowtie structure could also induce Bloch mode of the SPPs, thus decreasing the group velocity and further contributing to the enhancement effect. For the monolayer graphene, the responsivity could reach 0.5

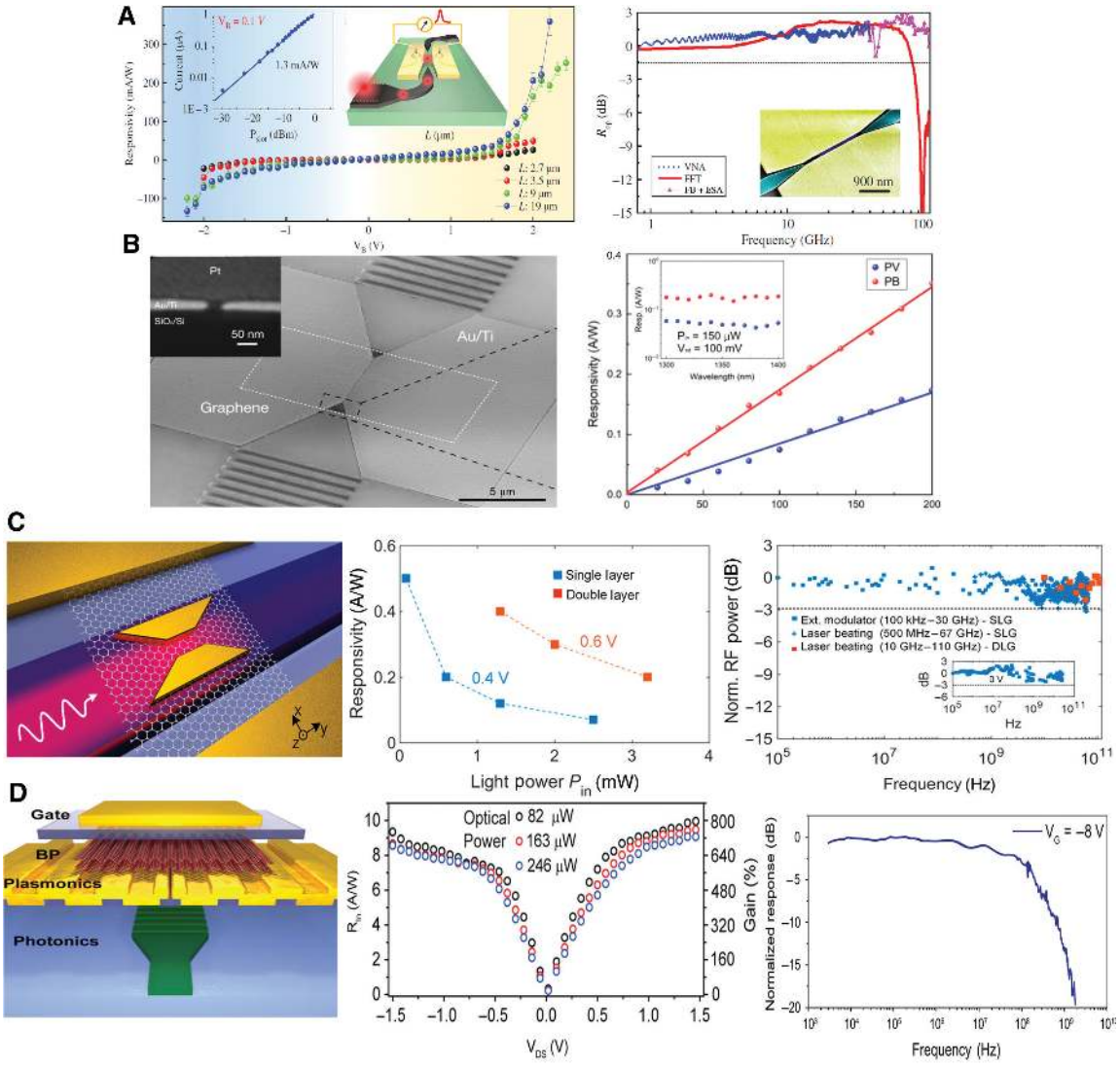

Figure 9: Plasmonically enhanced photodetectors based on the waveguide.
(A) Ultracompact graphene plasmonic photodetector on Si platform. The gap of the plasmonic slot is 120 nm. Pd and Ti are employed as contact with graphene to induce effective band bending. The maximum measured responsivity and bandwidth are 360 mA/W and 110 GHz, respectively. (B) Plasmonic photodetector with the metal slot width of 15 nm. The responsivity based on PV and PB effect are 0.35 A/W and 0.17 A/W. (C) Plasmonic photodetector based on bowtie nanostructure. When the input light power is 80 μW, the responsivity could reach up to 0.5 A/W. The bandwidth is larger than 110 GHz. (D) Black phosphorous photodetector with three-dimensional integration scheme. An intrinsic responsivity as high as 10 A/W and a 3-dB roll-off frequency of 150 MHz are experimentally demonstrated. Reproduced/adapted with permission from Ding et al. [35] (A), Ma et al. [220] (B), Ma et al. [221] (C), and Chen et al. [222] (D).

A/W for the input power of 80 μW. When the input power was further increased, both Joule heating and Pauli blocking significantly reduced the responsivity of the device. On the other hand, the double-layer graphene device could handle high input power without the saturation effect, maintaining the high responsivity of 0.4 A/W with the input power of 1.3 mW. The measured frequency response of devices was fairly good, showing a flat response covering from 100 kHz to 110 GHz. Moreover, the wavelength-dependent responsivity of the device was checked, exhibiting the flat response covering from S-band, C-band, to L-band of the optical communications. Considering the responsivity, bandwidth, and the footprint, this work could be one of the best photodetectors based on the plasmonic nanostructure integrated with 2D materials so far.

Black phosphorus could be another promising material in terms of photodetection owing to its direct and tunable bandgap, as well as the high sensitivity in the near- and mid-infrared regimes [224–226]. Black phosphorus analogs, such as Bi, Te, and SnS, have also been

Table 1: Summary of waveguide-type photodetectors using different waveguide and 2D material.

Reference	2D material	Main structure	Responsivity (A/W)	Bandwidth (GHz)
Gan et al. [229]	Exfoliated graphene	Si strip waveguide	0.1	20
Wang et al. [163]	Exfoliated graphene	Si suspended membrane waveguide	0.13	Not mentioned
Pospischil et al. [230]	Exfoliated graphene	Si strip waveguide	0.05	18
Schall et al. [231]	CVD graphene	Si strip waveguide	0.007	41
Youngblood et al. [232]	CVD graphene	Si strip waveguide	0.057	3
Shiue et al. [233]	Exfoliated graphene and hBN	Si strip waveguide	0.36	42
Schuler et al. [234]	Exfoliated graphene	Si slot waveguide	0.076	65
Flöry et al. [235]	vdWs heterostructure	Si strip waveguide	0.2	27
Goykhman et al. [236]	CVD graphene	Si–Au Schottky structure	0.37	Not mentioned
Ding et al. [35]	CVD graphene	Plasmonic slot waveguide	0.36	>110
Ma et al. [221]	CVD graphene	Si_3N_4 strip waveguide with metallic bowtie structures	0.5	>110
Guo et al. [237]	CVD graphene	Si-plasmonic hybrid waveguide	0.4	>40
Chen et al. [222]	Exfoliated BP	Si-plasmonic 3D integration	10	0.150

applied in the photodetection, but with moderate responsivity and response speed [196, 227, 228]. Multiple works of the BP photodetector based on both free-space and waveguide-integrated schemes were reported. Similar to graphene, these devices still suffer from low responsivity as well as large footprint. To address these issues, Chen et al. [222] proposed a hybrid plasmonic BP photodetector consisting of three different layers with different functionalities (Figure 9D). The bottom layer is a standard silicon-on-insulator platform, which transmits the light into the detection region with ultralow propagation loss. The plasmonic layer in the middle converts the photonic signal into the SPPs wave, concentrating light into the nanogap. The top layer is formed by an exfoliated BP flake as well as the top gating. Based on simulation results, up to 1% photonic emission from the waveguide was transmitted through the nanogap. The high responsivity of 10 A/W was measured in the device without the top gate when the applied bias was 1.5 V. The extremely high photoresponsivity could attribute to both the plasmonically enhanced light absorption, as well as the large gain factor owing to the charge trapping and short transit time within the structure. However, the RC constant severely limits the frequency response of the device, showing 3-dB bandwidth of only 150 MHz. Further optimization regarding the contact resistance, parasite capacitance could be valuable, but also challenging, in order to boost the frequency response while maintaining high responsivity of the proposed device.

Compared with the top-illumination photodetectors, the waveguide-type photodetectors show better performance in terms of large bandwidth, and they are also favorable for the integration with other on-chip optoelectronic devices. Here we summarize recent progress with respect to 2D-based waveguide-type photodetectors (Table 1). Thanks to metallic nanostructures, it is clearly seen, for example, in [35, 221], that photodetectors with plasmonic nanostructures hold much larger bandwidth as well as higher responsivity when compared to pure silicon waveguides. The better performance of these 2D material plasmonic hybrid photodetectors really takes advantages of plasmonic-enhanced light–matter interactions, and the miniaturization of plasmonic waveguide also gives rise to short drift paths for carriers in the photodetection region, resulting in large bandwidth. The chemical vapor deposition (CVD) graphene is widely exploited for integrated devices, thus allowing for mass production. Moreover, various 2D materials besides graphene, such as BP and vdWs heterostructure, have also been exploited with impressive performance. We believe that these developments will further the 2D materials toward practical applications, for example, in optical interconnects, high-speed optical communication, and so on.

4 Perspectives and conclusion

2D materials have shown to be a promising material for optoelectronic devices with performance enhanced by metallic nanostructures. The intrinsic weak light–matter interaction in 2D materials is greatly boosted by the polaritons using metallic nanostructures, and consequently the modulation depth and the responsivity of the photodetector can be significantly enhanced. Although the polaritons supported by 2D materials can also increase the light–matter interactions, most 2D polaritons work at longer wavelength, thus resulting in the challenge for the optoelectronic applications in the visible or near-infrared

window. For the 2D plasmonic hybrid devices, e.g. plasmonic-waveguide photodetectors [35], the ultrahigh speed has been achieved, while having extremely high insertion loss including high coupling loss between off-chip fiber to on-chip waveguide and from on-chip Si waveguide to plasmonic waveguide and the large propagation loss in the plasmonic waveguide. One might optimize the plasmonic waveguide geometry to increase the contribution of effect by the 2D material, e.g. narrowing plasmonic slot waveguide [35], which however might increase the challenge of nanofabrication and effective coupling. For particular plasmonic waveguide, such as the plasmonic slot waveguide, it is also challenging to realize precise alignment during nanofabrication, thus eventually ruining the performance. Some particular plasmonic waveguide design, for example, horizontal plasmonic slot waveguides might alleviate the requirement of alignment precision [238]. In this review, we have focused on discussing 2D material plasmonic hybrid systems for applications in electro-optical modulators and photodetectors. The intrinsic weak light–matter interaction in graphene is greatly boosted by the plasmonic structures; thus, the modulation depth of the modulator and the responsivity of the photodetector have also been enhanced. Further works regarding improving the light–matter interaction could be implemented with novel photonic structures, such as photonic crystal [166], high-quality factor microcavity [239], pure plasmonic circuit with low loss [240], or combination with 2D metallic materials [241]. Another important application of all-optical modulators or switches can also benefit a lot from metallic structures. Li et al. [178] reported all-optical switch based on saturation absorption of graphene on nanofiber with response time of 2.2 ps but extremely high power of 25 W (corresponding to 5.8 pJ switching energy with 220-fs pulse width). Ono et al. [160] found that with the plasmonic–graphene hybrid waveguide the switching energy can be significantly reduced to 35 fJ with much faster response time of 260 fs, thanks to the extremely enhanced light–matter interaction in the plasmonic waveguide.

Besides the wide investigation of individual 2D material–based optoelectronic devices, another important research field is to study a full on-chip interconnect link integrating all necessary 2D devices on a single chip. Youngblood et al. [232] first demonstrated integration of 2D material modulators and detectors on a single chip with GHz. Given the performances of the state-of-the-art 2D material modulators and photodetectors as discussed above, the on-chip interconnect with broad systematic bandwidth more than 30 GHz can be expected, which can be very useful for data centers. Another anticipated advantage of 2D plasmonic devices is simple fabrication process, making it easy to integrate modulators, photodetectors, and other optoelectronic devices on a single chip. On the other hand, most graphene-based 2D devices [30–32] mentioned above rely on wet transfer technology and other 2D material–based devices [92, 224] by mechanical exfoliation. The wet transfer process often leads to severe chemical contamination, affecting the electronic and optical properties, and the mechanical exfoliation is not suitable for mass production. These problems really call for the development of new technologies, including wafer-scale dry transfer technology for 2D materials, as well as new growth technology for other large-scale 2D materials. With the advances in these technologies, wafer-scale process of chips with 2D materials can be foreseen, taking the benefit from the mature Si technology. Moreover, the combination of 2D materials and metallic nanostructures could also play an important role in other areas besides communication, such as efficient water purification by enhancing the photothermal conversion [242, 243].

In summary, we have reviewed broad spectra of fundamentals and optoelectronic applications of 2D materials, where the light–matter interactions are extremely enhanced by metallic nanostructures. By taking advantages of strong localized field and subwavelength features of SPP, Raman signal, PL, nonlinear enhancement, and quantum features in 2D materials have been discussed. Then we have summarized the latest development of 2D material–based optoelectronic devices integrated with plasmonic nanostructures, and the performances of these optoelectronic devices can be greatly improved by metallic nanostructures, paving a promising way to realize 2D materials plasmonic hybrid optoelectronic devices for future optical interconnects.

Acknowledgment: The work is supported by the Center for Silicon Photonics for Optical Communication (SPOC, DNRF123, Funder Id: http://dx.doi.org/10.13039/501100001732) and the Center for Nanostructured Graphene (CNG, DNRF103, Funder Id: http://dx.doi.org/10.13039/501100001732) both sponsored by the Danish National Research Foundation. S.X. acknowledges the support from Independent Research Fund Denmark (Project No. 9041-00333B, Funder Id: http://dx.doi.org/10.13039/501100004836). Y.D. acknowledges the support from the QUANPIC project sponsored by VILLUM FONDEN (ref. 00025298) and mid-chip project sponsored by VILLUM FONDEN (No. 13367). X.Z. acknowledges the support of VILLUM Experiment (grant no. 17400) from VILLUM FONDEN.

References

[1] Haastrup S, Strange M, Pandey M, et al. The computational 2D materials database: high-throughput modeling and discovery of atomically thin crystals. 2D Mater 2018;5:042002.

[2] Novoselov KS, Geim AK, Morozov SV, et al. Electric field effect in atomically thin carbon films. Science 2004;306:666–9.

[3] Coleman JN, Lotya M, O'Neill A, et al. Two-dimensional nanosheets produced by liquid exfoliation of layered materials. Science 2011;331:568–71.

[4] Shen J, He Y, Wu J, et al. Liquid phase exfoliation of two-dimensional materials by directly probing and matching surface tension components. Nano Lett 2015;15:5449–54

[5] Tang S, Wang H, Wang H, et al. Silane-catalysed fast growth of large single-crystalline graphene on hexagonal boron nitride. Nat Commun 2015;6:6499.

[6] Xu X, Zhang Z, Qiu L, et al. Ultrafast growth of single-crystal graphene assisted by a continuous oxygen supply. Nat Nanotechnol 2016;11:930–5

[7] Wu T, Zhang X, Yuan Q, et al. Fast growth of inch-sized single-crystalline graphene from a controlled single nucleus on Cu-Ni alloys. Nat Mater 2016;15:43–7.

[8] Duan X, Wang C, Shaw JC, et al. Lateral epitaxial growth of two-dimensional layered semiconductor heterojunctions. Nat Nanotechnol 2014;9:1024–30.

[9] Novoselov KS, Mishchenko A, Carvalho A, Castro Neto AH. 2D materials and van der Waals heterostructures. Science 2016;353:aac9439.

[10] Pizzocchero F, Gammelgaard L, Jessen BS, et al. The hot pick-up technique for batch assembly of van der Waals heterostructures. Nat Commun 2016;7:11894.

[11] Cao Y, Fatemi V, Fang S, et al. Unconventional superconductivity in magic-angle graphene superlattices. Nature 2018;556:43–50.

[12] Cao Y, Fatemi V, Demir A, et al. Correlated insulator behaviour at half-filling in magic-angle graphene superlattices. Nature 2018;556:80–4.

[13] Tran K, Moody G, Wu F, et al. Evidence for Moire excitons in van der Waals heterostructures. Nature 2019;567:71–5.

[14] Karni O, Barre E, Lau SC, et al. Infrared interlayer exciton emission in MoS_2/WSe_2 heterostructures. Phys Rev Lett 2019;123:247402.

[15] Liu Y, Fang H, Rasmita A, et al. Room temperature nanocavity laser with interlayer excitons in 2D heterostructures. Sci Adv 2019;5:eaav4506.

[16] Paik EY, Zhang L, Burg GW, Gogna R, Tutuc E, Deng H. Interlayer exciton laser of extended spatial coherence in atomically thin heterostructures. Nature 2019;576:80–4.

[17] Saraswat KC, Mohammadi F. Effect of scaling of interconnects on the time delay of VLSI circuits. IEEE Trans Electron Devices 1982;4:645–50.

[18] Miller DA. Device requirements for optical interconnects to silicon chips. Proc IEEE 2009;97:1166–85.

[19] Zhang Y, Lim CK, Dai Z, et al. Photonics and optoelectronics using nano-structured hybrid perovskite media and their optical cavities. Phys Rep 2019;795:1–51.

[20] Tsai H, Nie W, Blancon JC, et al. High-efficiency two-dimensional Ruddlesden–Popper perovskite solar cells. Nature 2016;536:312–6.

[21] Blancon J-C, Tsai H, Nie W, et al. Extremely efficient internal exciton dissociation through edge states in layered 2D perovskites. Science 2017;355:1288–92.

[22] Xiao Z, Kerner RA, Zhao L, et al. Efficient perovskite light-emitting diodes featuring nanometre-sized crystallites. Nat Photon 2017;11:108.

[23] Saliba M, Wood SM, Patel JB, et al. Structured organic–inorganic perovskite toward a distributed feedback laser. Adv Mater 2016;28:923–9.

[24] Yang X, Cheng C, Wang Y, Qiu L, Li D. Liquid-mediated dense integration of graphene materials for compact capacitive energy storage. Science 2013;341:534–7.

[25] Wu W, Wang L, Li Y, et al. Piezoelectricity of single-atomic-layer MoS_2 for energy conversion and piezotronics. Nature 2014;514:470–4.

[26] Zhao M, Zhang J, Gao N, et al. Actively tunable visible surface plasmons in bi2te3 and their energy-harvesting applications. Adv Mater 2016;28:3138–44.

[27] Anasori B, Lukatskaya MR, Gogotsi Y. 2D metal carbides and nitrides (mxenes) for energy storage. Nat Rev Mater 2017;2:16098.

[28] Xia F, Wang H, Xiao D, Dubey M, Ramasubramaniam A. Two-dimensional material nanophotonics. Nat Photon 2014;8:899–907.

[29] Bonaccorso F, Sun Z, Hasan T, Ferrari AC. Graphene photonics and optoelectronics. Nat Photon 2010;4:611–22.

[30] Liu M, Yin X, Ulin-Avila E, et al. A graphene-based broadband optical modulator. Nature 2011;474:64–7.

[31] Phare CT, Yoon-Ho Lee D, Cardenas J, Lipson M. Graphene electro-optic modulator with 30 GHz bandwidth. Nat Photon 2015;9:511–4.

[32] Ding Y, Zhu X, Xiao S, et al. Effective electro-optical modulation with high extinction ratio by a graphene-silicon microring resonator. Nano Lett 2015;15:4393–400.

[33] Mueller T, Xia F, Avouris P. Graphene photodetectors for high-speed optical communications. Nat Nanotechnol 2010;4:297.

[34] Ding Y, Guan X, Zhu X, et al. Efficient electro-optic modulation in low-loss graphene–plasmonic slot waveguides. Nanoscale 2017;9:15576–81.

[35] Ding Y, Chen Z, Zhu X, et al. Ultra-compact integrated graphene plasmonic photodetector with bandwidth over 110 GHz. Nanophotonics 2020;9:317–25.

[36] Rodrigo D, Limaj O, Janner D, et al. Mid-infrared plasmonic biosensing with graphene. Science 2015;349:165–8.

[37] Rodrigo D, Tittl A, Limaj O, García de Abajo FJ, Pruneri V, Altug H. Double-layer graphene for enhanced tunable infrared plasmonics. Light Sci Appl 2017;6:e16277.

[38] Dontschuk N, Stacey A, Tadich A, et al. A graphene field-effect transistor as a molecule-specific probe of DNA nucleobases. Nat Commun 2015;6:6563.

[39] Hu H, Yang X, Zhai F, et al. Far-field nanoscale infrared spectroscopy of vibrational fingerprints of molecules with graphene plasmons. Nat Commun 2016;7:12334.

[40] Chen X, Park YJ, Kang M, et al. CVD-grown monolayer MoS_2 in bioabsorbable electronics and biosensors. Nat Commun 2018;9:1690.

[41] Hu H, Yang X, Guo X, et al. Gas identification with graphene plasmons. Nat Commun 2019;10:1131.

[42] Basov DN, Fogler MM, Garca de Abajo FJ. Polaritons in van der Waals materials. Science 2016;354:aag1992.

[43] Low T, Chaves A, Caldwell JD, et al. Polaritons in layered two-dimensional materials. Nat Mater 2017;16:182–94.
[44] Balandin AA, Nika DL. Phononics in low-dimensional materials. Mater Today 2012;15:266–75.
[45] Koppens FHL, Chang DE, Garca de Abajo FJ. Graphene plasmonics: A platform for strong light–matter interactions. Nano Lett 2011;11:3370–7.
[46] Britnell L, Ribeiro RM, Eckmann A, et al. Strong light–matter interactions in heterostructures of atomically thin films. Science 2013;340:1311–4.
[47] Liu X, Galfsky T, Sun Z, et al. Strong light–matter coupling in two-dimensional atomic crystals. Nat Photon 2015;9:30–4.
[48] Xiao S, Zhu X, Li B-H, Mortensen NA. Graphene-plasmon polaritons: From fundamental properties to potential applications. Front Phys 2016;11:117801.
[49] Zhu X, Wang W, Yan W, et al. Plasmon–phonon coupling in large-area graphene dot and antidot arrays fabricated by nanosphere lithography. Nano Lett 2014;14:2907–13.
[50] Gonçalves PAD, Peres NMR. An introduction to graphene plasmonics, 1st ed. Singapore: World Scientific, 2016.
[51] Dai S, Fei Z, Ma Q, et al. Tunable phonon polaritons in atomically thin van der Waals crystals of boron nitride. Science 2014;343:1125–29.
[52] Li P, Lewin M, Kretinin AV, et al. Hyperbolic phonon–polaritons in boron nitride for near-field optical imaging and focusing. Nat Commun 2015;6:7507.
[53] Wang G, Chernikov A, Glazov MM, et al. Colloquium: Excitons in atomically thin transition metal dichalcogenides. Rev Mod Phys 2018;90:021001.
[54] Liu W, Lee B, Naylor CH, et al. Strong exciton–plasmon coupling in MoS_2 coupled with plasmonic lattice. Nano Lett 2016;16:1262–9.
[55] Geisler M, Cui X, Wang J, et al. Single-crystalline gold nanodisks on WS_2 mono-and multilayers for strong coupling at room temperature. ACS Photonics 2019;6:994–1001.
[56] Zheng D, Zhang S, Deng Q, Kang M, Nordlander P, Xu H. Manipulating coherent plasmon–exciton interaction in a single silver nanorod on monolayer WSe_2. Nano Lett 2017;17:3809–14.
[57] Gonçalves PAD, Stenger N, Cox JD, Mortensen NA, Xiao S. Strong light–matter interactions enabled by polaritons in atomically thin materials. Adv Opt Mater 2020;8:201901473.
[58] Schuller JA, Barnard ES, Cai W, Jun YC, White JS, Brongersma ML. Plasmonics for extreme light concentration and manipulation. Nat Mater 2010;9:193–204.
[59] Li Y, Kang M, Shi J, Wu K, Zhang S, Xu H. Transversely divergent second harmonic generation by surface plasmon polaritons on single metallic nanowires. Nano Lett 2017;17:7803–8.
[60] Bauch M, Toma K, Toma M, Zhang Q, Dostalek J. Plasmon-enhanced fluorescence biosensors: a review. Plasmonics 2014;9:781–99.
[61] Zhu X, Xie F, Shi L, et al. Broadband enhancement of spontaneous emission in a photonic-plasmonic structure. Opt Lett 2012;37:2037–9.
[62] Moskovits M. Surface-enhanced Raman spectroscopy: a brief retrospective. J Raman Spectrosc 2005;36:485–96.
[63] Xu H, Aizpurua J, Käll M, Apell P. Electromagnetic contributions to single-molecule sensitivity in surface-enhanced Raman scattering. Phys Rev E 2000;62:4318–24.
[64] Hou W, Cronin SB. A review of surface plasmon resonance–enhanced photocatalysis. Adv Funct Mater 2013;23:1612–9.
[65] Kale MJ, Avanesian T, Christopher P. Direct photocatalysis by plasmonic nanostructures. ACS Catal 2014;4:116–28.
[66] Naldoni A, Riboni F, Guler U, Boltasseva A, Shalaev VM, Kildishev AV. Solar-powered plasmon-enhanced heterogeneous catalysis. Nanophotonics 2016;5:112–33.
[67] Cai W, Vasudev AP, Brongersma ML. Electrically controlled nonlinear generation of light with plasmonics. Science 2011;333:1720–3.
[68] Wurtz GA, Pollard R, Hendren W, et al. Designed ultrafast optical nonlinearity in a plasmonic nanorod metamaterial enhanced by nonlocality. Nat Nanotechnol 2011;6:106–10.
[69] Kauranen M, Zayats AV. Nonlinear plasmonics. Nat Photon 2012;6:737–48.
[70] Zhang Y, Wen F, Zhen P, Nordlander Y, Halas NJ. Coherent Fano resonances in a plasmonic nanocluster enhance optical four-wave mixing. Proc Natl Acad Sci U S A 2013;110:9215–9.
[71] Purdie DG, Popa D, Wittwer VJ, et al. Few-cycle pulses from a graphene mode-locked all-fiber laser. Appl Phys Lett 2015;106:253101.
[72] Song Y, Shi X, Wu C, Tang D, Zhang H. Recent progress of study on optical solitons in fiber lasers. Appl Phys Rev 2019;6:021313.
[73] Cushing SK, Wu N. Progress and perspectives of plasmon-enhanced solar energy conversion. J Phys Chem Lett 2016;7:666–75.
[74] Thomann I, Pinaud BA, Chen Z, Clemens BM, Jaramillo TF, Brongersma ML. Plasmon enhanced solar-to-fuel energy conversion. Nano Lett 2011;11:3440–6.
[75] Li J, Cushing SK, Meng F, Senty TR, Bristow AD, Wu N. Plasmon-induced resonance energy transfer for solar energy conversion. Nat Photon 2015;9:601.
[76] Gramotnev DK, Bozhevolnyi SI. Plasmonics beyond the diffraction limit. Nat Photon 2010;4:83–91.
[77] Echtermeyer TJ, Britnell L, Jasnos PK, et al. Strong plasmonic enhancement of photovoltage in graphene. Nat Commun 2011;2:458.
[78] Maier SA, Brongersma ML, Kik PG, Meltzer S, Requicha AAG, Atwater HA. Plasmonics–a route to nanoscale optical devices. Adv Mater 2001;13:1501–5.
[79] Bozhevolnyi S, Volkov VS, Devaux E, Laluet JY, Ebbesen TW. Channel plasmon subwavelength waveguide components including interferometers and ring resonators. Nature 2006;440:508–11.
[80] Oulton RF, Sorger VJ, Genov DA, Pile DFP, Zhang X. A hybrid plasmonic waveguide for subwavelength confinement and long-range propagation. Nat Photon 2008;2:496–500.
[81] Zia R, Schuller A, Chandran A, Brongersma ML. Plasmonics: the next chip-scale technology. Mater Today 2006;9:20–7.
[82] Ebbesen TW, Genet C, Bozhevolnyi SI. Surface-plasmon circuitry. Phys Today 2008;61:44–50.
[83] Fang Y, Sun M. Nanoplasmonic waveguides: towards applications in integrated nanophotonic circuits. Light Sci Appl 2015;4:e294.
[84] Nair RR, Blake P, Grigorenko AN, et al. Fine structure constant defines visual transparency of graphene. Science 2008;320:1308.
[85] Barnes WL, Dereux A, Ebbesen TW. Surface plasmon subwavelength optics. Nature 2003;424:824–30.
[86] Fleischmann M, Hendra PJ, McQuillan AJ. Raman spectra of pyridine adsorbed at a silver electrode. Chem Phys Lett 1974;26:163–6.

[87] Ferrari AC, Meyer JC, Scardaci V, et al. Raman spectrum of graphene and graphene layers. Phys Rev Lett 2006;97:187401.
[88] Zhu X, Shi L, Schmidt MS, et al. Enhanced light–matter interactions in graphene-covered gold nanovoid arrays. Nano Lett 2013;13:4690–6.
[89] Thareja V, Esfandyarpour M, Kik PG, Brongersma ML. Anisotropic metasurfaces as tunable SERS substrates for 2D materials. ACS Photon 2019;6:1996–2004.
[90] Celano U, Maccaferri N. Chasing plasmons in flatland. Nano Lett 2019;19:7549–52.
[91] Heeg S, Fernandez-Garcia R, Oikonomou A, et al. Polarized plasmonic enhancement by au nanostructures probed through Raman scattering of suspended graphene. Nano Lett 2013;13:301–8.
[92] Chen W, Zhang S, Kang M, et al. Probing the limits of plasmonic enhancement using a two-dimensional atomic crystal probe. Light Sci Appl 2018;7:56.
[93] Ling X, Fang W, Lee YH, et al. Raman enhancement effect on two-dimensional layered materials: graphene, h-BN and MoS_2. Nano Lett 2014;14:3033–40.
[94] Anderson MS. Locally enhanced Raman spectroscopy with an atomic force microscope. Appl Phys Lett 2000;76:3130–2.
[95] Zhang R, Zhang Y, Dong ZC, et al. Chemical mapping of a single molecule by plasmon-enhanced Raman scattering. Nature 2013;498:82–86.
[96] Zhu W, Esteban R, Borisov AG, et al. Quantum mechanical effects in plasmonic structures with subnanometre gaps. Nat Commun 2016;7:11495.
[97] Sigle DO, Hugall JT, Ithurria S, Dubertret B, Baumberg JJ. Probing confined phonon modes in individual CdSe nanoplatelets using surface-enhanced Raman scattering. Phys Rev Lett 2014;113:087402.
[98] Splendiani A, Sun L, Zhang Y, et al. Emerging photoluminescence in monolayer MoS_2. Nano Lett 2010;10:1271–5.
[99] Ye Y, Wong ZJ, Lu X, et al. Monolayer excitonic laser. Nat Photon 2015;9:733–737.
[100] Wu S, Buckley S, Schaibley JR, et al. Monolayer semiconductor nanocavity lasers with ultralow thresholds. Nature 2015;520:69–72.
[101] Salehzadeh O, Djavid M, Tran NH, Shih I, Mi Z. Optically pumped two-dimensional MoS_2 lasers operating at room-temperature. Nano Lett 2015;15:5302–6.
[102] Butun S, Tongay S, Aydin K. Enhanced light emission from large-area monolayer MoS_2 using plasmonic nanodisc arrays. Nano Lett 2015;15:2700–4.
[103] Gong SH, Alpeggiani F, Sciacca B, Garnett EC, Kuipers L. Nanoscale chiral valley-photon interface through optical spin-orbit coupling. Science 2018;359:443–7.
[104] Li Z, Liu C, Rong X, et al. Tailoring MoS_2 valley-polarized photoluminescence with super chiral near-field. Adv Mater 2018;30:1801908.
[105] Xu X, Yao W, Xiao D, Heinz TF. Spin and pseudospins in layered transition metal dichalcogenides. Nat Phys 2014;10:343–50.
[106] Srivastava A, Sidler M, Allain AV, Lembke DS, Kis A, Imamoglu A. Valley Zeeman effect in elementary optical excitations of monolayer WSe_2. Nat Phys 2015;11:141–7.
[107] Yu N, Capasso F. Flat optics with designer metasurfaces. Nat Mater 2014;13:139–50.
[108] Sun L, Wang C, Krasnok A, et al. Separation of valley excitons in a MoS_2 monolayer using a subwavelength asymmetric groove array. Nat Photon 2019;13:180–4.
[109] Bao Q, Zhang H, Wang Y, et al. Atomic-layer graphene as a saturable absorber for ultrafast pulsed lasers. Adv Funct Mater 2009;19:3077–83.
[110] Sun Z, Hasan T, Torrisi F, et al. Graphene mode-locked ultrafast laser. ACS Nano 2010;4:803–10.
[111] Wang Z, Dong Z, Zhu H, et al. Selectively plasmon-enhanced second-harmonic generation from monolayer tungsten diselenide on flexible substrates. ACS Nano 2018;12:1859–67.
[112] Hu G, Hong X, Wang K, et al. Coherent steering of nonlinear chiral valley photons with a synthetic au-ws2 metasurface. Nat Photon 2019;13:467–72.
[113] Guo T, Jin B, Argyropoulos C. Hybrid graphene–plasmonic gratings to achieve enhanced nonlinear effects at terahertz frequencies. Phys Rev Appl 2019;11:024050.
[114] Diaconescu B, Pohl K, Vattuone L, et al. Low-energy acoustic plasmons at metal surfaces. Nature 2007;448:57–9.
[115] Principi A, Asgari R, Polini M. Acoustic plasmons and composite hole-acoustic plasmon satellite bands in graphene on a metal gate. Solid State Commun 2011;151:1627–30.
[116] Gu X, Lin IT, Liu J. Extremely confined terahertz surface plasmon-polaritons in graphene–metal structures. Appl Phys Lett 2013;103:071103.
[117] Alonso-González P, Nikitin AY, Gao Y, et al. Acoustic terahertz graphene plasmons revealed by photocurrent nanoscopy. Nat Nanotechnol 2017;12:31–5.
[118] Lundeberg MB, Gao Y, Asgari R, et al. Tuning quantum nonlocal effects in graphene plasmonics. Science 2017;357:187–91.
[119] Alcaraz Iranzo D, Nanot S, Dias EJC, et al. Probing the ultimate plasmon confinement limits with a van der Waals heterostructure. Science 2018;360:291–5.
[120] Chen J, Badioli M, Alonso-González P, et al. Optical nano-imaging of gate-tunable graphene plasmons. Nature 2012;487:77–81.
[121] Fei Z, Rodin AS, Andreev GO, et al. Gate-tuning of graphene plasmons revealed by infrared nano-imaging. Nature 2012;487:82–5.
[122] Lundeberg MB, Gao Y, Woessner A, et al. Thermoelectric detection and imaging of propagating graphene plasmons. Nat Mater 2017;16:204–7.
[123] Dias EJC, Iranzo DA, Gonçalves PAD, et al. Probing nonlocal effects in metals with graphene plasmons. Phys Rev B 2018;97:245405.
[124] Rodríguez Echarri A, Joel Cox D, Javier García de Abajo F. Quantum effects in the acoustic plasmons of atomically thin heterostructures. Optica 2019;6:630–41.
[125] Woessner A, Lundeberg MB, Gao Y, et al. Highly confined low-loss plasmons in graphene–boron nitride heterostructures. Nat Mater 2015;14:421–5.
[126] Wang L, Meric I, Huang PY, et al. One-dimensional electrical contact to a two-dimensional material. Science 2013;342:614–7.
[127] Andrews JG, Buzzi S, Choi W, et al. What will 5G be? IEEE J Sel Area Comm 2014;32:1065–82.
[128] Wu G, Talwar S, Johnsson K, Himayat N, Johnson KD. M2M: from mobile to embedded internet. IEEE Commun. Mag 2011;49:36–43.

[129] Agrawal GP. Fiber-optic communication systems, Volume 222. Hoboken, NJ, USA, John Wiley & Sons, 2012.
[130] Essiambre RJ, Kramer G, Winzer PJ, Foschini GJ, Goebel B. Capacity limits of optical fiber networks. J Light Technol 2010;28:662–701.
[131] Essiambre RJ, Tkach RW. Capacity trends and limits of optical communication networks. Proc IEEE 2012;100:1035–55.
[132] Duan X, Huang Y, Agarwal R, Lieber CM. Single-nanowire electrically driven lasers. Nature 2003;421:241–245.
[133] Park H, Fang AW, Kodama S, Bowers JE. Hybrid silicon evanescent laser fabricated with a silicon waveguide and III-V offset quantum well. Opt Express 2005;13:9460–4.
[134] Xu Q, Schmidt B, Pradhan S, Lipson M. Micrometre-scale silicon electro-optic modulator. Nature 2005;435:325–7.
[135] Colace L, Masini G, Assanto G, Luan H, Wada K, Kimerling LC. Efficient high-speed near-infrared Ge photodetectors integrated on Si substrates. Appl Phys Lett 2000;76:1231–3.
[136] Roelkens G, Van Thourhout D, Baets R, Notzel R, Smit M. Laser emission and photodetection in an InP/InGaAsP layer integrated on and coupled to a silicon-on-insulator waveguide circuit. Opt Express 2006;14:8154–9.
[137] Miller DAB. Device requirements for optical interconnects to silicon chips. Proc IEEE 2009;97:1166–85.
[138] Uenuma M, Moooka T. Temperature-independent silicon waveguide optical filter. Opt Lett 2009;34:599–601.
[139] Dong J, Liu L, Gao D, et al. Compact notch microwave photonic filters using on-chip integrated microring resonators. IEEE Phtonics J 2013;5:5500307.
[140] Baehr-Jones T, Hochberg M, Walker C, Scherer A. High-Q optical resonators in silicon-on-insulator–based slot waveguides. Appl Phys Lett 2005;86:081101.
[141] Vlasov Y, Green WMJ, Xia F. High-throughput silicon nanophotonic wavelength-insensitive switch for on-chip optical networks. Nat Photon 2008;2:242–6.
[142] Chen L, Chen Y-K. Compact, low-loss and low-power 8×8 broadband silicon optical switch. Opt Express 2012;20:18977–85.
[143] Lu L, Zhao S, Zhou L, et al. 16×16 Non-blocking silicon optical switch based on electro-optic Mach-Zehnder interferometers. Opt Express 2016;24:9295–307.
[144] Lee H, Chen T, Li J, Painter O, Vahala KJ. Ultra-low-loss optical delay line on a silicon chip. Nat Commun 2012;3:867.
[145] Cardenas J, Foster MA, Sherwood-Droz N, et al. Wide-bandwidth continuously tunable optical delay line using silicon microring resonators. Opt Express 2010;18:26525–34.
[146] Wang X, Zhou L, Li R, et al. Continuously tunable ultra-thin silicon waveguide optical delay line. Optica 2017;4:507–15.
[147] Reed GT, Mashanovich G, Gardes FY, Thomson DJ. Silicon optical modulators. Nat Photon 2010;4:518–26.
[148] Liu PQ, Valmorra F, Maissen C, Faist J. Electrically tunable graphene anti-dot array terahertz plasmonic crystals exhibiting multi-band resonances. Optica 2015;2:135–40.
[149] Timurdogan E, Sorace-Agaskar CM, Sun J, Hosseini ES, Biberman A, Watts MR. An ultralow power athermal silicon modulator. Nat Commun 2014;5:1–11.
[150] Baba T, Akiyama S, Imai M, et al. 50-gb/s ring-resonator-based silicon modulator. Opt Express 2013;21:11869–76.
[151] Alexander K, George JP, Verbist J, et al. Nanophotonic pockels modulators on a silicon nitride platform. Nat Commun 2018;9:3444.
[152] Chen S, Li W, Wu J, et al. Electrically pumped continuous-wave III–V quantum dot lasers on silicon. Nat Photon 2016;10:307–11.
[153] Wang Z, Van Gasse K, Moskalenko V, et al. A III-V-on-Si ultra-dense comb laser. Light Sci Appl 2017;6:e16260.
[154] Wan Y, Zhang Z, Chao R, et al. Monolithically integrated InAs/InGaAs quantum dot photodetectors on silicon substrates. Opt Express 2017;25:27715–23.
[155] Gibson SJ, van Kasteren B, Tekcan B, et al. Tapered InP nanowire arrays for efficient broadband high-speed single-photon detection. Nat Nanotechnol 2019;14:473–9.
[156] Li S, Xu L, Zhao S. 5g internet of things: a survey. J. Industrial Information Integration 2018;110:1–9.
[157] Werner S, Navaridas J, Luján M. A survey on optical network-on-chip architectures. ACM Comput Surv 2017;50:1–37.
[158] Russell SJ, Norvig P. Artificial intelligence: a modern approach. Malaysia: Pearson Education Limited, 2016.
[159] Bolotin KI, Sikes KJ, Jiang Z, et al. Ultrahigh electron mobility in suspended graphene. Solid State Commun 2008;146:351–5.
[160] Ono M, Hata M, Tsunekawa M, et al. Ultrafast and energy-efficient all-optical switching with graphene-loaded deep-subwavelength plasmonic waveguides. Nat Photon 2020;14:37–43.
[161] Zeng B, Huang Z, Singh A, et al. Hybrid graphene metasurfaces for high-speed mid-infrared light modulation and single-pixel imaging. Light Sci Appl 2018;7:1–8.
[162] Guo X, Wang W, Nan H, et al. Ni. High-performance graphene photodetector using interfacial gating. Optica 2016;3:1066–70.
[163] Wang X, Cheng Z, Xu K, Tsang HK, Xu J-B. High-responsivity graphene/silicon-heterostructure waveguide photodetectors. Nat Photon 2013;7:888–91.
[164] Dufferwiel S, Schwarz S, Withers F, et al. Exciton–polaritons in van der Waals heterostructures embedded in tunable microcavities. Nat Commun 2015;6:8579.
[165] Furchi M, Urich A, Pospischil A, et al. Microcavity-integrated graphene photodetector. Nano Lett 2012;12:2773–7.
[166] Yan S, Zhu X, Frandsen LH, et al. Slow-light-enhanced energy efficiency for graphene microheaters on silicon photonic crystal waveguides. Nat Commun 2017;8:14411.
[167] Zhou H, Gu T, McMillan JF, et al. Enhanced four-wave mixing in graphene-silicon slow-light photonic crystal waveguides. Appl Phys Lett 2014;105:091111.
[168] Liu M, Yin X, Zhang X. Double-layer graphene optical modulator. Nano Lett 2012;12:1482–5.
[169] Melikyan A, Alloatti L, Muslija A, et al. High-speed plasmonic phase modulators. Nat Photon 2014;8:229–33.
[170] He C, Pan S, Guo R, Zhao Y, Pan M. Ultraflat optical frequency comb generated based on cascaded polarization modulators. Opt Lett 2012;37:3834–6.
[171] Soref R, Bennett B. Electrooptical effects in silicon. IEEE J. Quantum Electron 1987;23:123–9.
[172] Cocorullo G, Rendina I. Thermo-optical modulation at 1.5 μm in silicon etalon. Electron Lett 1992;28:83–5.
[173] Miller DAB, Chemla DS, Schmitt-Rink S. Relation between electroabsorption in bulk semiconductors and in quantum wells: the quantum-confined Franz–Keldysh effect. Phys Rev B 1986;33:6976–82.
[174] Miller DAB, Chemla DS, Damen TC, et al. Band-edge electroabsorption in quantum well structures: the quantum-confined stark effect. Phys Rev Lett 1984;53:2173–6.

[175] Sato K. Measurement of magneto-optical Kerr effect using piezo-birefringent modulator. Jpn J Appl Phys 1981;20:2403.
[176] Lemme MC, Echtermeyer TJ, Baus M, et al. Mobility in graphene double gate field effect transistors. Solid State Electron 2008;52:514–8.
[177] Wang F, Zhang Y, Tian C, et al. Gate-variable optical transitions in graphene. Science 2008;320:206–9.
[178] Li W, Chen B, Meng C, et al. Ultrafast all-optical graphene modulator. Nano Lett 2014;14:955–9.
[179] Sorianello V, Midrio M, Contestabile G, et al. Graphene–silicon phase modulators with gigahertz bandwidth. Nat Photon 2018;12:40–4.
[180] Yu S, Wu X, Chen K, et al. All-optical graphene modulator based on optical Kerr phase shift. Optica 2016;3:541–4.
[181] Mak KF, Ju L, Wang F, Heinz TF. Optical spectroscopy of graphene: from the far infrared to the ultraviolet. Solid State Commun 2012;152:1341–9.
[182] Dalir H, Xia Y, Wang Y, Zhang X. Athermal broadband graphene optical modulator with 35 GHz speed. ACS Photonics 2016;3:1564–8.
[183] Yan H, Li X, Chandra B, et al. Tunable infrared plasmonic devices using graphene/insulator stacks. Nat Nanotechnol 2012;7:330–4.
[184] Qian H, Ma Y, Yang Q, et al. Electrical tuning of surface plasmon polariton propagation in graphene–nanowire hybrid structure. ACS Nano 2014;8:2584–9.
[185] Kim J, Son H, Cho DJ, et al. Electrical control of optical plasmon resonance with graphene. Nano Lett 2012;12:5598–602.
[186] Emani NK, Chung T-F, Ni X, Kildishev AV, Chen YP, Boltasseva A. Electrically tunable damping of plasmonic resonances with graphene. Nano Lett 2012;12:5202–6.
[187] Emani NK, Chung T-F, Kildishev AV, Shalaev VM, Chen YP, Boltasseva A. Electrical modulation of Fano resonance in plasmonic nanostructures using graphene. Nano Lett 2014;14:78–82.
[188] Yao Y, Shankar R, Kats MA, et al. Electrically tunable metasurface perfect absorbers for ultrathin mid-infrared optical modulators. Nano Lett 2014;14:6526–32.
[189] Ansell D, Radko IP, Han Z, Rodriguez FJ, Bozhevolnyi SI, Grigorenko AN. Hybrid graphene plasmonic waveguide modulators. Nat Commun 2015;6:8846.
[190] Klein M, Badada BH, Binder R, et al. 2D semiconductor nonlinear plasmonic modulators. Nat Commun 2019;10:3264.
[191] Mak KF, Lee C, Hone J, Shan J, Heinz TF. Atomically thin MoS_2 2: a new direct-gap semiconductor. Phys Rev Lett 2010;105:136805.
[192] Back P, Zeytinoglu S, Ijaz A, Kroner M, Imamoğlu A. Realization of an electrically tunable narrow-bandwidth atomically thin mirror using monolayer MoS_2e_2. Phys Rev Lett 2018;120:037401.
[193] Chen Y, Jiang G, Chen S, et al. Mechanically exfoliated black phosphorus as a new saturable absorber for both Q-switching and mode-locking laser operation. Opt Express 2015;23:12823–33.
[194] Lu S, Miao L, Guo Z, et al. Broadband nonlinear optical response in multi-layer black phosphorus: an emerging infrared and mid-infrared optical material. Opt Express 2015;23:11183–94.
[195] Huang W, Li C, Gao L, et al. Emerging black phosphorus analogue nanomaterials for high-performance device applications. J Mater Chem C 2020;8:1172–97.
[196] Li C, Huang W, Gao L, et al. Recent advances in solution-processed photodetectors based on inorganic and hybrid photo-active materials. Nanoscale 2020;12:2201–27.
[197] Wang Y, Huang W, Wang C, et al. An all-optical, actively q-switched fiber laser by an antimonene-based optical modulator. Laser Photon Rev 2019;13:1800313.
[198] Peng R, Chen C, Li M. Broadband waveguide integrated black phosphorus modulator for mid infrared application. In: CLEO: Science and Innovations. Washington, DC, USA, Optical Society of America, 2018:SM2B-3.
[199] Emsley MK, Dosunmu O, Unlu MS. High-speed resonant-cavity–enhanced silicon photodetectors on reflecting silicon-on-insulator substrates. IEEE Photon Technol Lett 2002;14:519–21.
[200] Chen E, Chou SY. High-efficiency and high-speed silicon metal–semiconductor–metal photodetectors operating in the infrared. Appl Phys Lett 1997;70:753–5.
[201] Huang Z, Carey JE, Liu M, Guo X, Mazur E, Campbell JC. Microstructured silicon photodetector. Appl Phys Lett 2006;89:033506.
[202] Ackert JJ, Thomson DJ, Shen L, et al. High-speed detection at two micrometres with monolithic silicon photodiodes. Nat Photon 2015;9:393.
[203] Tang L, Kocabas SE, Latif S, et al. Nanometre-scale germanium photodetector enhanced by a near-infrared dipole antenna. Nat Photon 2008;2:226–9.
[204] Vivien L, Osmond J, Fédéli J-M, et al. 42 GHz pin germanium photodetector integrated in a silicon-on-insulator waveguide. Opt Express 2009;17:6252–7.
[205] Michel J, Liu J, Kimerling LC. High-performance Ge-on-Si photodetectors. Nat Photon 2010;4:527–34.
[206] Liao S, Feng N-N, Feng D, et al. 36 GHz submicron silicon waveguide germanium photodetector. Opt Express 2011;19:10967–72.
[207] Vivien L, Polzer A, Marris-Morini D, et al. Zero-bias 40GBit/s germanium waveguide photodetector on silicon. Opt Express 2012;20:1096–101.
[208] Chen H, Galili M, Verheyen P, et al. 100-Gbps RZ data reception in 67-GHz Si-contacted germanium waveguide pin photodetectors. J Light Technol 2016;35:722–726.
[209] Park H, Fang AW, Jones R, et al. A hybrid algainas-silicon evanescent waveguide photodetector. Opt Express 2007;15:6044–52.
[210] Monroy E, Calle F, Pau JL, et al. Algan-based UV photodetectors. J Cryst Growth 2001;230:537–43.
[211] Sheng Z, Liu L, Brouckaert J, He S, Van Thourhout D. InGaAs pin photodetectors integrated on silicon-on-insulator waveguides. Opt Express 2010;18:1756–61.
[212] Bean JC. Silicon-based semiconductor heterostructures: column IV bandgap engineering. Proc IEEE 1992;80:571–87.
[213] Xia F, Mueller T, Lin Y-M, Valdes-Garcia A, Avouris P. Ultrafast graphene photodetector. Nat Nanotechnol 2009;4:839.
[214] Fang Z, Liu Z, Wang Y, Ajayan PM, Nordlander P, Halas NJ. Graphene-antenna sandwich photodetector. Nano Lett 2012;12:3808–13.
[215] Sun T, Wang Y, Yu W, et al. Flexible broadband graphene photodetectors enhanced by plasmonic $Cu_{3-x}P$ colloidal nanocrystals. Small 2017;13:1701881.
[216] Blauth M, Vest G, Rosemary SL, et al. Ultracompact photodetection in atomically thin $MoSe_2$. ACS Photonics 2019;6:1902–9.

[217] Ni Z, Ma L, Du S, et al. Plasmonic silicon quantum dots enabled high-sensitivity ultrabroadband photodetection of graphene-based hybrid phototransistors article. ACS Nano 2017;11:9854–62.
[218] Amani M, Lien D-H, Kiriya D, et al. A. Near-unity photoluminescence quantum yield in MoS_2. Science 2015;350:1065–8.
[219] Kim JT, Yu Y-J, Choi H, and Choi C-G. Graphene-based plasmonic photodetector for photonic integrated circuits. Opt Express 2014;22:803.
[220] Ma Z, Kikunage K, Wang H, et al. Compact graphene plasmonic slot photodetector on silicon-on-insulator with high responsivity. 2018, arXiv preprint arXiv:1812.00894.
[221] Ma P, Salamin Y, Baeuerle B, et al. Plasmonically enhanced graphene photodetector featuring 100 GBit/s data reception, high responsivity, and compact size. ACS Photonics 2019;6:154–61.
[222] Chen C, Youngblood N, Peng R, et al. Three-dimensional integration of black phosphorus photodetector with silicon photonics and nanoplasmonics. Nano Lett 2017;17:985–91.
[223] Muench JE, Ruocco A, Giambra MA, et al. Waveguide-Integrated, Plasmonic Enhanced Graphene Photodetectors. Nano Lett 2019;19:7632–44.
[224] Li L, Yu Y, Ye GJ, et al. Black phosphorus field-effect transistors. Nat Nanotechnol 2014;9:372.
[225] Das S, Zhang W, Demarteau M, Hoffmann A, Dubey M, Roelofs A. Tunable transport gap in phosphorene. Nano Lett 2014;14:5733–9.
[226] Engel M, Steiner M, Avouris P. Black phosphorus photodetector for multispectral, high-resolution imaging. Nano Lett 2014;14:6414–7.
[227] Huang W, Xie Z, Fan T, et al. Black-phosphorus-analogue tin monosulfide: an emerging optoelectronic two-dimensional material for high-performance photodetection with improved stability under ambient/harsh conditions. J Mater Chem C 2018;6:9582–93.
[228] Huang W, Xing C, Wang Y, et al. Facile fabrication and characterization of two-dimensional bismuth (III) sulfide nanosheets for high-performance photodetector applications under ambient conditions. Nanoscale 2018;10:2404–12.
[229] Gan X, Shiue RJ, Gao Y, et al. Chip-integrated ultrafast graphene photodetector with high responsivity. Nat Photon 2013;7:883.
[230] Pospischil A, Humer M, Furchi MM, et al. CMOS-compatible graphene photodetector covering all optical communication bands. Nat Photon 2013;7:892–6.
[231] Schall D, Neumaier D, Mohsin M, et al. 50 GBit/s photodetectors based on wafer-scale graphene for integrated silicon photonic communication systems. ACS Photonics 2014;1:781–4.
[232] Youngblood N, Anugrah Y, Ma R, Koester SJ, Li M. Multifunctional graphene optical modulator and photodetector integrated on silicon waveguides. Nano Lett 2014;14:2741–6.
[233] Shiue R-J, Gao Y, Wang Y, et al. High-responsivity graphene–boron nitride photodetector and autocorrelator in a silicon photonic integrated circuit. Nano Lett 2015;15:7288–93.
[234] Schuler S, Schall D, Neumaier D, et al. Controlled generation of a p–n junction in a waveguide integrated graphene photodetector. Nano Lett 2016;16:7107–112.
[235] Flöry N, Ma P, Salamin Y, et al. Waveguide-integrated van der Waals heterostructure photodetector at telecom wavelengths with high speed and high responsivity. Nat Nanotechnol 2020;15:118–24.
[236] Goykhman I, Sassi U, Desiatov B, et al. On-chip integrated, silicon–graphene plasmonic Schottky photodetector with high responsivity and avalanche photogain. Nano Lett 2016;16:3005–13.
[237] Guo J, Li J, Liu C, et al. High-performance silicon- graphene hybrid plasmonic waveguide photodetectors beyond 1.55 μm. Light Sci Appl 2020;9:1–11.
[238] Huang T, Shao X, Shum PP, et al. Internal asymmetric plasmonic slot waveguide for third harmonic generation with large fabrication tolerance. Plasmonics 2016;11:1451–9.
[239] Armani D, Kippenberg T, Spillane S, Vahala K. Ultra-high-Q toroid microcavity on a chip. Nature 2003;421:925–8.
[240] Salamin Y, Ma P, Baeuerle B, et al. 100 GHz plasmonic photodetector. ACS Photon 2018;5:3291–7.
[241] Xie Z, Chen S, Duo Y, et al. Biocompatible two-dimensional titanium nanosheets for multimodal imaging-guided cancer theranostics. ACS Appl Mater Interfaces 2019;11:22129–40.
[242] Xie Z, Peng Y, Yu L, et al. Solar-inspired water purification based on emerging 2D materials: status and challenges. Solar RRL 2020;4:1900400.
[243] Xie Z, Duo Y, Lin Z, et al. The rise of 2D photothermal materials beyond graphene for clean water production. Adv Sci 2020;7:1902236.